Plant Science 336 (2023) 111833

Contents lists available at ScienceDirect

Plant Science

journal homepage: www.elsevier.com/locate/plantsci

# Thylakoid membrane appression in the giant chloroplast of *Selaginella martensii* Spring: A lycophyte challenges grana paradigms in shade-adapted species

Andrea Colpo [a], Alessandra Molinari [b], Paola Boldrini [c], Marek Živčak [d], Marian Brestič [d], Sara Demaria [a], Costanza Baldisserotto [a], Simonetta Pancaldi [a], Lorenzo Ferroni [a,*]

[a] Department of Environmental and Prevention Sciences, University of Ferrara, Corso Ercole I d'Este 32, 44121 Ferrara, Italy
[b] Department of Chemical, Pharmaceutical and Agricultural Sciences, University of Ferrara, Via Luigi Borsari 46, 44121 Ferrara, Italy
[c] Center of Electron Microscopy, University of Ferrara, Via Luigi Borsari 46, 44121 Ferrara, Italy
[d] Department of Plant Physiology, Faculty of Agrobiology and Food Resources, Slovak University of Agriculture, A. Hlinku 2, Nitra, 949 76, Slovak Republic

ARTICLE INFO

*Keywords:*
Grana
Lycophyte
Shade-adaptation
Thylakoid
Ultrastructure

ABSTRACT

In vascular plants, the thylakoid architecture is dominated by the highly structured multiple membrane layers known as grana. The structural diversity of the thylakoid system among plant species is mainly determined by the adaptation to the growth light regime, according to a paradigm stating that shade-tolerant species are featured by a high membrane extension with an enhanced number of thylakoid layers per granum. In this study, the thylakoid system was analysed in *Selaginella martensii* Spring, a shade-adapted rainforest species belonging to lycophytes, a diminutive plant lineage, sister clade of all other vascular plants (euphyllophytes, including ferns and seed plants). The species is characterized by giant cup-shaped chloroplasts in the upper epidermis and, quantitatively less important, disk-shaped chloroplasts in the mesophyll and lower epidermis. The study aimed at the quantitative assessment of the thylakoid appression exploiting a combination of complementary methods, including electron microscopy, selective thylakoid solubilisation, electron paramagnetic resonance, and simultaneous analysis of fast chlorophyll *a* fluorescence and P700 redox state. With a chlorophyll *a/b* ratio of 2.6 and PSI/PSII ratio of 0.31, the plant confirmed two typical hallmarks of shade-adaptation. The morphometric analysis of electron micrographs revealed a 33% fraction of non-appressed thylakoid domains. However, contrasting with the structural paradigm of thylakoid shade-adaptation in angiosperms, *S. martensii* privileges the increase in the granum diameter in place of the increase in the number of layers building the granum. The very wide grana diameter, 727 nm on average, largely overcame the threshold of 500 nm currently hypothesized to allow an effective diffusion of long-range electron carriers. The fraction of non-appressed membranes based on the selective solubilisation of thylakoids with digitonin was 26%, lower than the morphometric determination, indicating the presence of non-appressed domains inaccessible to the detergent, most probably because of the high three-dimensional complexity of the thylakoid system in *S. martensii*. Particularly, strong irregularity of grana stacks is determined by assembling thylakoid layers of variable width that tend to slide apart from each other as the number of stacked layers increases.

## 1. Introduction

Selaginellaceae, with the only genus *Selaginella*, are a rich family of lycophytes, the diminutive early divergent group of vascular plants, sister clade of the euphyllophytes (Weststrand and Korall, 2016). Most *Selaginella* species are found in the lower vegetation layers of tropical and subtropical forests, where the plant life would be impossible without special adaptations to deep shade. Light reaches the understory after having been attenuated by the upper canopy, which not only strongly reduces irradiance, but also modifies the spectral composition of the light available to photosynthesis, determining a relative enrichment in green and far-red wavelengths. Moreover, understory plants are exposed to unpredictable fluctuations in both light intensity and quality because of the sunflecks filtering through the canopy. The

* Corresponding author.
*E-mail address:* lorenzo.ferroni@unife.it (L. Ferroni).

https://doi.org/10.1016/j.plantsci.2023.111833
Received 11 March 2023; Received in revised form 17 July 2023; Accepted 15 August 2023
Available online 17 August 2023

morphological adaptations of species adapted to deep shade are known for some time and include all levels of biological organization from the plant habit to the leaf anatomy, from the cell shape to the thylakoid system architecture inside the chloroplasts (Anderson et al., 1988; Kozlowski and Pallardy, 1997; Mathur et al., 2018).

The most characterizing morphological feature of the thylakoid system is the segregation of the membranes into granal and stromal lamellar domains, which is biochemically related to the uneven distribution of photosystem I (PSI) in the stroma-exposed domains and photosystem II (PSII) in the appressed domains (Andersson and Anderson, 1980). A granum can be defined as an approximately cylindrical stack with a diameter of ca. 400–600 nm and formed by at least three thylakoids, usually 5–25, depending on species and light conditions (Mazur et al., 2021; Rantala et al., 2020). Magnificent three-dimensional renderings of the granum structure and its connections with the stroma lamellae are currently available for model angiosperms (Austin and Staehelin, 2011; Bussi et al., 2019; Mustárdy et al., 2008a; for a historical review on thylakoid architecture modelling, see Staehelin and Paolillo, 2020). However, the almost perfect cylindrical stack is more an exception than the rule, because grana show various degrees of irregularity related to different diameters of the thylakoid layers and shifting of the layers in the lateral plane (Brangeon and Mustárdy, 1979; Mustárdy and Garab, 2003; Mazur et al. 2021). The thylakoid stacking depends on three main factors (Mustárdy et al., 2008b): as a precondition, the sorting of PSII and its light-harvesting complex LHCII from the other complexes due to lateral interactions leading to the formation of various types of PSII-LHCII megacomplexes and (semi-)crystalline lattices (Dekker and Boekema, 2005, Garab, 2016); the vertical interactions of the supramolecular complexes formed by PSII and LHCII in the appressed regions (Barber, 1980, Chow et al. 2005, Albanese et al. 2020); the exclusion of PSI and the ATP synthase from the grana cores because of their stromal protrusions, which cannot be accommodated in the stromal gap of the grana partitions (Daum et al., 2010; Miller and Staehelin, 1976; Nevo et al., 2012). The regions found at the interface between the appressed and non-appressed domains are called the "grana margins" (Rantala et al., 2020). The grana curvature areas are another thylakoid domain enriched in membrane curvature factors, which regulate the granum size (Armbruster et al., 2013; Trotta et al., 2019). Inside the chloroplasts of shade-adapted plants, particularly angiosperms, the thylakoid system is very abundant, and the grana stacks are irregularly orientated and made up of several tens of thylakoids, even up to hundreds (e.g., *Alocasia macrorrhiza*, Anderson et al. 1973; *Anoectochilus roxburghii*, Shao et al., 2014; *Monstera deliciosa*, Demmig-Adams et al. 2015). The large amount of LHCII compared to PSII typically leads to low chlorophyll (Chl) *a/b* molar ratios (2.3–2.7) compared to sun-adapted plants (2.9–3.6; Lichtenthaler and Babani, 2004, Anderson et al. 2012). Given the exclusion of PSI from the grana cores and the need of understory plants for balancing the over-excitation of PSI due to the enrichment in far-red light, a high degree of thylakoid appression is expectedly accompanied by a low PSI/PSII ratio (Pantaleoni et al., 2009; Schöttler and Tóth, 2014; Walters and Horton, 1994).

Broadening the perspective to non-angiosperms, the structural diversity of the chloroplasts in shade plants is not limited to the size of the grana stacks. The striking ultrastructural shade adaptations in *Selaginella* species are instructive of an evolution of shade-adaptation traits that occurred independently of that better-characterized in angiosperms (Liu et al., 2020; Sheue et al., 2007). In the very small and thin microphylls of rainforest *Selaginella* species the upper epidermal cells are usually the main location of photosynthesis (Ferroni et al., 2016; Jagels, 1970; Sheue et al., 2007). The upper epidermal cells are roughly conical and, in many species, host only one giant chloroplast per cell, generally lying at the cell bottom to collect as much light as possible through a very extensive thylakoid system (Liu et al. 2020). Light harvesting is helped by the convex upper tangential cell wall, sometimes ornamented with silica bodies, which focuses light downwards to the chloroplast (lens effect; Liu et al. 2020; Shih et al., 2022). At the same time, the funnel-shape of the cell allows multiple light reflections inside the protoplast to possibly enable light harvesting also by less exposed thylakoids (light-pipe effect; Liu et al. 2020). In the *Selaginella* species adapted to the deepest shade (subgenus *Stachygynandrum*, Liu et al. 2020), the thylakoid system can differentiate into two structural zones, an upper region with parallel long lamellae formed by 2–4 appressed thylakoids and a lower granal structure (Ferroni et al., 2016; Liu et al., 2020; Sheue et al., 2007, 2015). In such "bizonoplast", the upper thylakoid lamellae are deemed responsible for blue iridescence, a phenomenon also observed in some deep-shade angiosperms, such as many *Begonia* species and *Phyllogatis rotundifolia* (Castillo et al., 2021; Gould and Lee, 1996; Masters et al., 2018; Pao et al., 2018). In the most characterized species *S. erythropus*, the lower chloroplast region contains grana formed on average by 18 stacked thylakoids with a diameter of ca. 600 nm (Sheue et al., 2007). Therefore, despite the adaptation to deep shade, the granal structure lays within common ranges of grana size variation with respect to the granum height, and at the upper limit of the granum diameter (Kirchhoff, 2019; Rantala et al., 2020). In the related species *S. martensii*, the upper epidermal cells host likewise a bizonoplast, although the thylakoid zonation is less pronounced than in *S. erythropus* (Ferroni et al. 2016) or can also lack (Liu et al. 2020). In the prevailing granal region, occupying a major part of the chloroplast, the thylakoid stacking degree appears very variable inside the same organelle (Ferroni et al. 2016).

Because a high degree of thylakoid stacking is a very characterising morphological trait in the cell biology of shade-adapted species, in this report we aimed at testing if this assumption can be supported quantitatively in *S. martensii*. The thylakoid stacking extent was analysed using complementary morphometric (electron microscopy) and biochemical (differential thylakoid solubilisation) approaches, in combination with the electron paramagnetic resonance determination of the PSI/PSII ratio and the in vivo simultaneous analysis of prompt Chl *a* fluorescence and PSI oxidation state.

## 2. Materials and Methods

### 2.1. Plant material

The plant material used in this research was sampled from a colony of *Selaginella martensii* Spring (Selaginellaceae) kept under stable environmental conditions in the warm humid greenhouse at the Botanical Garden of the University of Ferrara (44°50′30″ N, 11°37′21″E). The temperature was maintained at 25–30 °C and the relative humidity was always above 60%. The greenhouse reproduces the natural shade of the lower vegetation layers in a dense forest formation, where the *S. martensii* plants grow in a low-intensity, far-red enriched environment. All over the year, the maximum incident light intensity is less than 80 μmol photons $m^{-2}$ $s^{-1}$ and is enriched in far red (red/far red quantum ratio, 0.7). For analyses, terminal branches (2–3 ramifications from the apex) were sampled at the end of the night and all manipulations were done under a dim green safe light.

### 2.2. Thylakoid isolation

For thylakoid isolation the protocol described in (Pantaleoni et al., 2009) was used with modifications as follows. At the end of the night, the terminal branches were cut and immediately transferred to a cold mortar (−20 °C). The cold (4 °C) grinding buffer was added (50 mM Tricine/KOH – pH 7.6, 330 mM sorbitol, 2 mM $Na_2EDTA$, 5 mM $MgCl_2$, 2.5 mM ascorbate, 0.05% bovine serum albumin, 10 mM NaF). After addition of sand quartz, the sample was quickly homogenized with a cold pestle and the homogenate was filtered through two layers of Miracloth (Calbiochem) and collected in a tube kept in ice. After centrifugation at 150 *g* for 5 min at 4 °C to remove cell debris and residual quartz, the supernatant was collected and centrifuged at 18.000 *g* for 5 min at 4 °C. The pellet, containing the chloroplasts, was subjected to hypoosmotic stress by resuspending in a cold shock buffer (50 mM

Tricine/KOH – pH 7.6, 5 mM sorbitol, 2 mM $Na_2EDTA$, 5 mM $MgCl_2$, 10 mM NaF). Centrifugation at 18.000 *g* for 5 min at 4 °C allowed to collect the isolated thylakoids in the pellet, which were resuspended in storage buffer (50 mM Tricine/KOH – pH 7.6, 100 mM sorbitol, 2 mM $Na_2EDTA$, 5 mM $MgCl_2$, 10 mM NaF) to a final Chl concentration of ca. 1–2 mg $mL^{-1}$. The Chl concentration in the thylakoid suspension was determined after extraction with 80% (v/v) buffered acetone (2.5 mM Hepes/NaOH, pH 7.5) and quantitated as described by Porra et al. (1989). Subsequently, the samples were stored in liquid nitrogen until used for analyses.

### 2.3. Electron paramagnetic resonance

The protocol for the detection of the PSI and PSII signals was adapted from Danielsson et al. (2004) and Fan et al. (2007). The isolated thylakoids were pelleted by centrifugation at 18.000 *g* at 4 °C for 5 min, the supernatant was discarded and the thylakoid pellet was resuspended with a MES [2-(N-morpholino)ethanesulfonic acid] buffer having the following composition: 15 mM MES/NaOH pH 6.5, 15 mM NaCl, 300 mM sucrose, to give a final Chl concentration of 3–4 mg $mL^{-1}$ in a volume of 250 μL inside a 1.5 mL microtube. The thylakoid suspension was maintained on ice in darkness and used for electron paramagnetic resonance (EPR) measurements.

For EPR measurements, a Bruker ER200 MRD spectrometer equipped with a TE201 resonator was used at the following conditions: frequency 9.76 GHz, power 39.65 mW, modulation frequency 100 kHz, modulation amplitude 5.00 G, time constant 163.84 ms, number of scans 8. The instrument was calibrated by using α,α'-diphenylpicrylhydrazyl (DPPH). The sample to be analyzed (250 μL) was put in a flat quartz cell and the EPR spectrum was recorded for the blank constituted by a 5 mM solution of $K_3[Fe(CN)_6]$ prepared in MES buffer. The radical-cation $P700^+$ in PSI (one radical spin per reaction centre) was chemically generated by addition of freshly prepared $K_3[Fe(CN)_6]$ to the thylakoid suspension to give a final concentration of 5 mM. After a dark incubation period of 10 min at room temperature, the sample was put in the flat cell for the EPR measurement of $P700^+$ signal. After the record, the flat cell was recovered from the cavity and exposed to white fluorescent light (ca. 30 μmol photons $m^{-2}$ $s^{-1}$) for 60 s at room temperature. Then, the cell was reinserted into the cavity for the detection of the light-induced, dark-stable Tyrosine D radical in PSII reaction centre ($Y_D^{\cdot}$, one radical spin per reaction centre). Readjustment of the resonance conditions in the cavity corresponded to a waiting time of ca. 5 min prior to $YD^{\cdot}$ signal registration. For spectra elaboration, Origin™ version 2022 (OriginLab, Northampton, MA, USA) was used. The $P700^+$ signal was obtained by subtracting the $K_3[Fe(CN)_6]$ blank signal to avoid the disturbance due to Fe. Because the $P700^+$ signal is a single narrow line (Fan et al. 2007), it was easily identified nearby the G value typical of radicals; a line was drawn manually intersecting the signal centre tangential to the basal outline in the neighbourhood of the $P700^+$ line. The drawn line was used as baseline for integration, thus assigning to the signal centre the value of zero in the derivative, i.e., the maximum in the resulting quasi-Gaussian primitive curve. The intensity of the PSI signal was determined as the area subtended under the latter curve. For PSII, the $Y_D^{\cdot}$ signal overlapped on that of $P700^+$ (+ $K_3[Fe(CN)_6]$) and therefore was obtained by subtraction. The derivative $Y_D^{\cdot}$ signal is larger than that of $P700^+$ and consists of composite lines (Fan et al. 2007), therefore giving rise to a complex primitive curve; nevertheless, the signal centre was recognizable, and the same analytical procedure was applied as per the $P700^+$ signal, obtaining the signal intensity of $Y_D^{\cdot}$. Both radical signals are equimolar to the respective photosystems, and the $Y_D^{\cdot}$/ $P700^+$ area ratio was used as an estimate of the PSII/PSI stoichiometry.

### 2.4. Comparative thylakoid solubilization

The methods used were adapted from (Rantala et al., 2017). Aliquots of thylakoid suspensions corresponding to 8 μg Chl were collected by centrifugation at 18.000 *g* for 5 min at 4 °C and the supernatant was discarded. The pellet was then treated in one of the three following alternatives for solubilisation, in all cases operating in very dim light.

(1) Solubilisation with β-dodecylmaltoside (β-DM; Sigma-Aldrich) in BTH buffer [25 mM BisTris/HCl – pH 7.0, 20% (w/v) glycerol, 0.25 mg $mL^{-1}$ Pefabloc, 10 mM NaF], on ice for 10 min with very slow mixing.
(2) Solubilisation with digitonin (Calbiochem) in BTH buffer, at room temperature (23 °C) for 30 min with continuous gentle mixing.
(3) Solubilisation with digitonin in ACA buffer [50 mM BisTris/HCl – pH 7.0, 375 mM e-aminocaproic acid, 1 mM $Na_2EDTA$, 0.25 mg $mL^{-1}$ Pefabloc, 10 mM NaF], at room temperature (23 °C) for 30 min with continuous gentle mixing.

Operatively, the pellets were first resuspended in the buffer (BTH or ACA) and an equal volume of detergent solution (in BTH or ACA buffer) was added to obtain the final detergent concentrations of 0 (insolubilized control), 0.75, 1.50, 2.50%. After solubilization, the insolubilized material was pelleted by centrifugation at 18.000 *g* at 4 °C for 20 min. The solubilized and insolubilized fractions were used to determine the respective Chl content as described in the previous paragraph. Alternatively, they were treated for SDS-PAGE separation of thylakoid proteins on a resolving gel with 15% acrylamide and 6 M urea (Laemmli, 1970). Gels were silver stained using routine protocols.

### 2.5. Simultaneous analysis of P700 redox state and Chl a fluorescence

A Dual PAM-100 (Walz, Germany) was used for the measurement of the fast Chl *a* fluorescence induction and the P700 redox state (Ferroni et al., 2022; Klughammer and Schreiber, 1994; Zivcak et al., 2014a). Uncut terminal branches of dark-acclimated plants were positioned in the measuring head of the instrument, allowing a further dark-acclimation for ca. 2 min before analysis. Subsequently, the sample was exposed to a 600 ms-long saturation pulse with intensity of 3.000 μmol photons $m^{-2}$ $s^{-1}$. During the pulse, the Chl *a* fluorescence emission signal and the $P700^+$ absorption signal (dual wavelength 830/875 nm) were recorded simultaneously at a high frequency (0.3 ms intervals).

### 2.6. Transmission electron microscopy

Small portions of branches sampled from four independent plants were cut and transferred into a 10-mL syringe. Soon after, 3 mL of a fixing solution were added (3% glutaraldehyde in 0.1 M K-Na phosphate buffer, pH 7.2, kept at 4 °C) and air in intercellular spaces was removed creating a slight vacuum with the syringe plunger. The syringe was then covered with aluminium foil and fixation was allowed for 4 h at room temperature. After several washings with phosphate buffer, the samples were recovered in a vial and post-fixed with 1% $OsO_4$ in the same buffer over night at 4 °C (Ferroni et al. 2016). After dehydration in a graded acetone series, the samples were infiltrated with Durcupan ACM epoxy resin. The ultrathin sections were contrasted with lead citrate and uranyl acetate and, for observation, a Zeiss EM910 transmission electron microscope was used (Electron Microscopy Centre, University of Ferrara).

For morphometric determinations of the thylakoid system, micrographs were analysed using the free processing package Fiji (https://imagej.net/software/fiji/). The measurements were performed on micrographs taken at 31.500 × corresponding to an observation field of 6.7 $\mu m^2$ (2.91 × 2.30 μm). From the four biological replicates, many sections for the morphometric analyses were examined. For the upper epidermis, one field was chosen per giant chloroplast to contain one to three grana stacks sectioned almost parallel to the vertical granum axis, for a total of 24 micrographs; in addition, ten micrographs were taken from mesophyll chloroplasts.

The granum morphometrics was performed according to Mazur et al. (2021). For the granum vertical perspective, all grana in each micrograph were analysed, even when not perfectly transversally sectioned. The granum height (*h*) was determined as the distance between the top and bottom layers of the granum end-membranes, taking into account variable diameters of the stack and lateral irregularities. Helped by the "Plot Profile" function of ImageJ, the number of thylakoid layers per granum (*N*) was determined in each case and the Stacking Repeat Distance (*SRD*) was calculated as:

$$SRD = h/N$$

For the horizontal perspective, the width of each appressed thylakoid layer in a granum was analysed only in complete, transversely sectioned grana stacks. The granum irregularity was quantified for the same grana using two parameters proposed by Kowalewska et al. (2016) and Mazur et al. (2021). The "Granum Lateral Irregularity" (*GLI*) is the coefficient of variation of membrane diameters within a single granum and was calculated as follows:

*GLI* = (Standard deviation of layer widths)/(Average of layers widths).

The "Granum Cross-Sectional Irregularity" (*GSI*) was used to quantify the shifting of the membranes on the lateral plane and was calculated by comparing the granum cross-sectional area ($A_G$) with that of the rectangle having the same height and perimeter of the granum ($A_R$):

$$GSI = (A_R\text{-}A_G)/A_R$$

For the determination of the degree of thylakoid appression in each observation field at 31.500 × , at first the density of thylakoid appression per granum surface unit ($\delta_{STACK}$, nm nm$^{-2}$) was calculated from the transversally sectioned grana using the width of the grana partitions:

$$\delta_{STACK} = \frac{\Sigma(width\quad of\quad partitions)}{A_G}$$

Applying the $\delta_{STACK}$ to all grana in a picture, the full length of the appressed membranes was calculated. The following equation was used to calculate the fraction of appressed membranes (the non-appressed membranes are the complement to one):

$$Relative\quad Appressed = \frac{2\delta_{STACK} \bullet \Sigma A_G}{2(\Sigma Stroma\quad thylakoids) + \Sigma Granum\quad perimeter + 2\delta_{STACK} \bullet \Sigma A_G}$$

Because not all grana in each picture were sectioned transversally, the use of estimates based on $\delta_{STACK}$ introduced an overestimation of the appressed domains, which was however deemed acceptable to the scope of the work. The appressed/non appressed membrane ratio was also calculated.

### 2.7. Statistical data treatment

For the statistical treatment of data, OriginPro version 2023b was used (OriginLab Corporation, Northampton, MA, USA). For the morphometrics, the software was used to draw histograms of relative frequencies and the corresponding normal distribution. To compare samples, Student's *t*-test was used with significance threshold fixed ad 0.05. The covariation of specific morphometric parameters was analysed with the Linear Fit tool of OriginPro.

## 3. Results

### 3.1. Chl a/b ratio and PSI/PSII ratio

The Chl *a*/*b* molar ratio is a very good absolute marker to define the shade adaptation degree of vascular plants and is inversely proportional to the relative abundance of LHCII (Anderson et al., 2012; Lichtenthaler and Babani, 2004). Shade-adapted plants have an expected Chl *a*/*b* ratio within a range of [2.3–2.8]. In buffered acetonic extracts, the Chl *a*/*b* ratio of *S. martensii* thylakoids, sampled in different periods of the year, was within the interval [2.43–2.85] with a mean of 2.63 ± 0.14 (SD, $n = 16$).

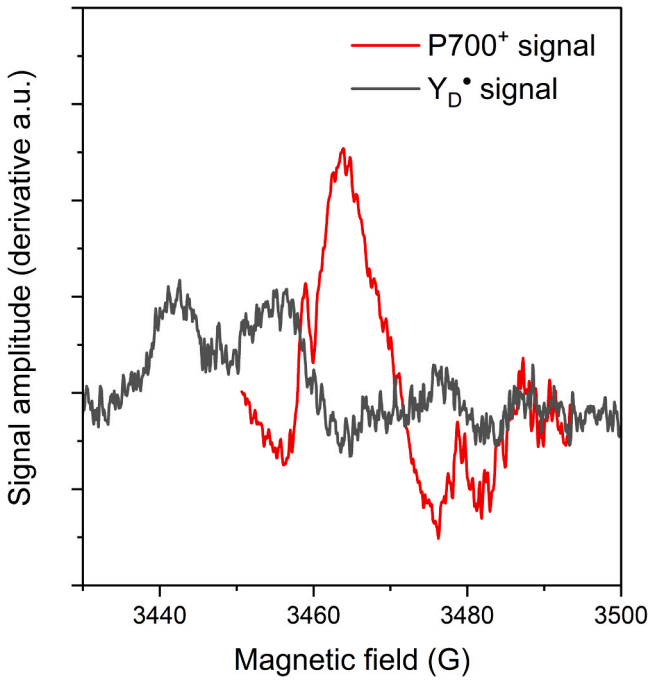


**Fig. 1.** Spectra of EPR signals associated with tyrosine D radical $Y_D^{\bullet}$ in PSII and $P700^+$ radical cation in PSI in thylakoids isolated from *Selaginella martensii*.

EPR spectroscopy is an elective method for the precise determination of the PSI/PSII reaction centre stoichiometry (Danielsson et al., 2004; Fan et al., 2007; Ermakova et al., 2021). Preliminarily to each replicate analysis, the region of DPPH resonance was centred at 3457 G. In general, operating at conditions comparable to the relevant literature, the EPR signals of photosystems in *S. martensii* thylakoids had an extremely low intensity, which was symptomatic of the low concentration of reaction centres in the thylakoid membranes. The $P700^+$ signal of PSI was a single line centred at ca. 3466 G; the $Y_D^{\bullet}$ signal was less defined and larger, centred at ca. 3462 G (Fig. 1). The average PSI/PSII ratio estimated from five independent biological replicates was 0.31 ± 0.04 (SE of the mean), indicating that PSII was in a large excess of PSI in *S. martensii* thylakoids. The value was similar to that reported in pea plants grown under far-red enriched light (ca. 0.4; Fan et al. 2007). Therefore, Chl *a*/*b* and PSI/PSII ratios were in line with the shade-adaptation of this species, particularly the abundance of antennae in response to a low light availability and the low amount of PSI in response to the enrichment in far red.

### 3.2. Fast Chl a fluorescence induction and P700 oxidation state

To obtain further information on the shade adaptation of *S. martensii*, we analysed the in vivo fast Chl *a* fluorescence transient (OJIP) upon the microphyll excitation with a saturating pulse. When visualized on a logarithmic timescale, the OJIP transient appears polyphasic: starting from a minimum value of fluorescence at step O, it shows a first fast increase up to an inflection at step J, followed by a second rise and a new inflection at step I, before reaching the plateau P, corresponding to the maximum fluorescence emitted by PSII (for review, Stirbet and Govindjee, 2011). In *S. martensii* the J and I steps were reached after approx. 4 and 40 ms from the onset of the pulse, respectively (Fig. 2A). The amplitude of relative fluorescence at I step ($\Delta V_{I\text{-}P}$) depends on the activity of PSI that moves electrons from the reduced intersystem electron carriers to its end acceptors (ferredoxin and

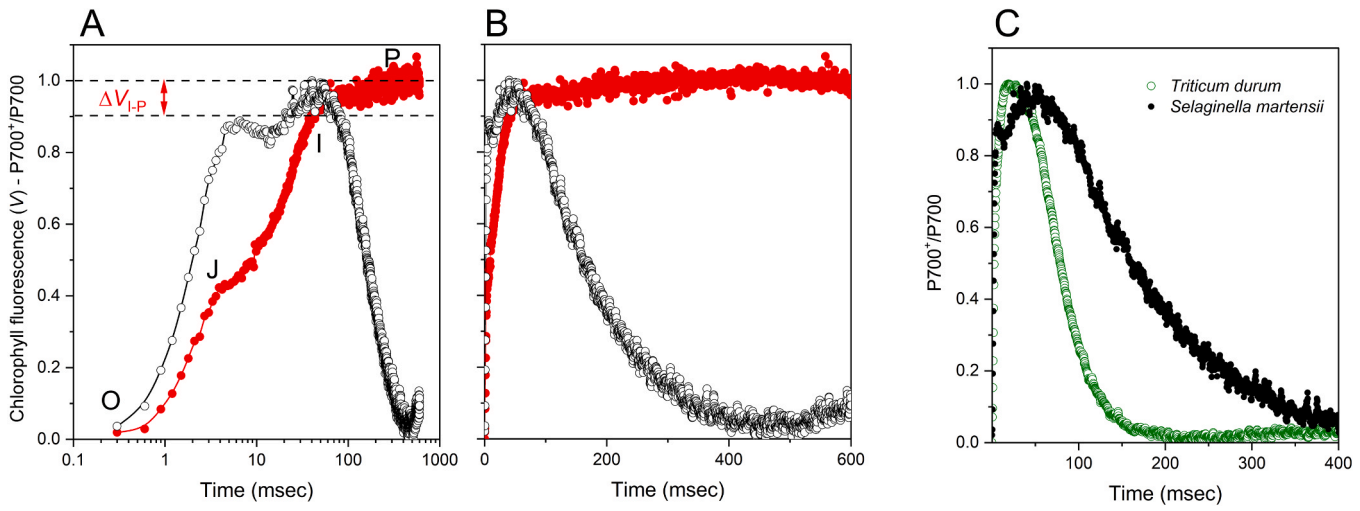


**Fig. 2.** Kinetics of chlorophyll *a* fluorescence induction and P700 oxidation kinetics in *Selaginella martensii* microphylls. (A) Simultaneous kinetics represented on a logarithmic timescale and double normalized between maximum and minimum. The noticeable steps of the fluorescence transient (red) are indicated as the origin O, the first inflection J, the second inflection I, and the final value P. The relative amplitude of the I-P phase is indicated as $\Delta V_{I\text{-}P}$. The P700 oxidation kinetics is shown in black. Notice that the I step marks the final rise of fluorescence and also the re-reduction of P700. (B) The same as in A, represented on a linear timescale. (C) Comparative P700 oxidation kinetics in *S. martensii* (green) and in *Triticum durum* (durum wheat, black). Notice the extremely slow re-reduction of P700 in the lycophyte.

ferredoxin-NADP$^+$-oxido-reductase) and is an indirect indicator of the PSI/PSII stoichiometry (Ceppi et al., 2012; Schansker et al., 2005; for relevant exceptions see Zivcak et al., 2015 and Ferroni et al., 2022). In seed plants, the value is generally within a range of [0.18–0.35] (e.g., Zivcak et al., 2014b; Pollastrini et al., 2016; 2020; Umar et al., 2019; Killi et al., 2020; Filacek et al., 2022). The OJIP transient of *S. martensii* was evidently characterized by a very small I-P amplitude: the $\Delta V_{I\text{-}P}$ value of 0.119 ± 0.009 (SE, $N = 5$) confirmed the low abundance of PSI relative to PSII.

We also analysed the changes in P700 oxidation state in PSI reaction centre simultaneous with the Chl fluorescence rise. During the first 3–4 ms, the P700$^+$ signal increased very rapidly nearly approaching its maximum (Fig. 2A). The cause for the P700$^+$ accumulation was the lack of reduced electron transporters during the O-J phase, which is dominated by the reduction of the primary electron acceptor $Q_A$ in PSII reaction centre, up to reaching a transitionary equilibrium with the $Q_A^-$ oxidation by forward electron transport to the plastoquinone pool at step J. Again, the very prompt and nearly complete oxidation of P700 in just a few ms was indicative of a small relative amount of PSI. During the subsequent J-I phase, the plastoquinone pool was progressively reduced (Tóth et al., 2007), starting to make electrons available to the re-reduction of P700 through the plastocyanin. In angiosperms, P700$^+$ still markedly accumulates during the J-I phase, approaching a transitionary steady state after 7–10 ms from the onset of the pulse — this testifies to an effective supply of electrons leading to a balance between P700 oxidation and re-reduction (Ferroni et al., 2022; Guo et al., 2020; Tsimilli-Michael, 2020; Zivcak et al., 2014a). In *S. martensii* the increase in P700$^+$ was instead marginal during the J-I phase and the maximum P700$^+$ (a quite sharp peak rather than a quasi-plateau) was reached in correspondence of the I step at ca. 40 ms (Fig. 2A). Subsequently, the complete re-reduction of P700$^+$ took approx. 350 ms, with the exhaustion of the oxidized end electron acceptors of PSI (Fig. 2B). For reference, in Fig. 2C, the P700$^+$ kinetics is shown comparatively in *S. martensii* and in the angiosperm *Triticum durum* (durum wheat), where the re-reduction of P700 was achieved in some 100–150 ms. Therefore, in *S. martensii*, the electrons were made very slowly available to the reduction of P700$^+$.

### 3.3. Differential solubilization of the thylakoid membranes

To simplify the characterization of the thylakoid system in *S. martensii* chloroplasts, the plant material was sampled at the end of the night, when the thylakoid system generally emphasizes the lateral heterogeneity of the photosynthetic complexes, i.e., a stricter segregation of PSII and PSI in grana cores or stroma-exposed domains, respectively (Rantala et al., 2020). The isolated thylakoid membranes were solubilized using three different mild detergents at three concentrations, following the rationale exposed by (Rantala et al., 2017).

β-DM is a very commonly used non-ionic detergent, releasing almost all protein complexes from the thylakoid membrane network (Aro et al., 2005; Järvi et al., 2011). This detergent is able to effectively penetrate the grana cores, destroying the weak hydrophobic interactions keeping together the LHCII lake with PSII and PSI (Grieco et al., 2015). β-DM in BTH buffer allows a quantitative and non-selective solubilization of thylakoids, and therefore it was used in this experiment as a control. In the absence of detergent, the BTH buffer alone did not lead to any measurable release of Chl-containing complexes. The solubilization yield, approaching 90%, did not differ significantly between the three β-DM concentrations, although slightly higher at 1.5% and 2.5%. (Fig. 3). The Chl *a*/*b* molar ratio was determined in the solubilized and non-solubilized fractions and their weighted means were compared for consistency with the Chl *a*/*b* ratio of the entire thylakoids of origin. Expectedly, the β-DM-solubilized fractions had a Chl *a*/*b* ratio very similar to that of the entire thylakoid system. The 10% non-solubilized fraction did not differ significantly from that of the solubilized fraction (Table 1).

In order to assess biochemically the degree of thylakoid appression, the thylakoids were treated with increasing concentrations of digitonin using the same BTH buffer as for β-DM. Digitonin is an amphipathic molecule as β-DM but is bulkier and cannot penetrate the grana cores, i.e., digitonin solubilizes only the stroma-exposed thylakoid domains (Järvi et al., 2011; Suorsa et al., 2015). With *S. martensii* thylakoids, the solubilization yield with digitonin in BTH buffer was approximately the same independent of the detergent concentration, on average 24% (Fig. 3). The mean Chl *a*/*b* ratio of the solubilized fraction was 3.2, significantly higher than 2.5 in the insoluble fraction (Student's *t* test, $P < 10^{-7}$), indicating the selective action of digitonin on the thylakoid

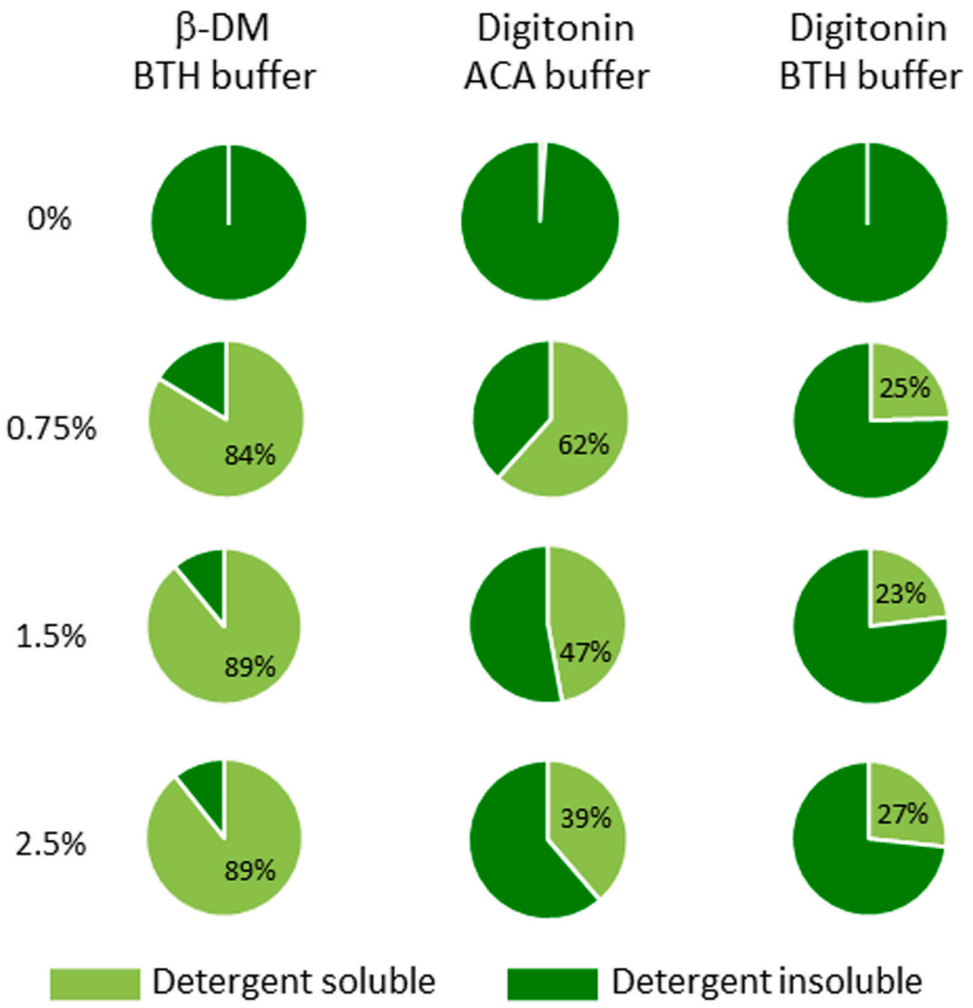


**Fig. 3.** Solubilization of thylakoids isolated from *Selaginella martensii* at the end of the night with different detergent treatments. Thylakoid membranes were solubilized with different concentrations of β-dodecyl maltoside (β-DM) in bis-tris-HCl (BTH) buffer, or digitonin in BTH, or digitonin in aminocaproic acid buffer (ACA). The insolubilized membranes were pelleted by centrifugation. The chlorophyll content was determined in solubilized fraction (detergent-soluble supernatant) and insolubilized fraction (detergent-insoluble pellet). Each diagram represents the mean of 3–5 independent replicates.

system, although the difference between the two ratios was relatively small, only 0.7 (Table 1). Particularly, the Chl *a/b* ratio in the insoluble fraction was in line with reported values of the grana core of angiosperms (ca. 2.5; Danielsson et al., 2004; Rantala et al., 2017, Koochak et al., 2019). Conversely, in the soluble fraction the 3.2 ratio was markedly lower than expected, i.e., ca. 4.5 reported in digitonin-solubilized stroma-exposed thylakoid domains of angiosperms (Danielsson et al., 2004; Rantala et al., 2017).

As a further control, the digitonin solubilization was carried out in ACA buffer. Rantala et al. reported that digitonin in ACA buffer can solubilize the entire thylakoid system with an efficiency comparable to that of β-DM, i.e., losing the selectivity of this detergent towards appressed and non-appressed domains (Rantala et al., 2017; 2022). As with BTH, ACA buffer alone did not lead to significant thylakoid solubilization. Different from expected, we could not reach ca. 90% solubilization as with β-DM and increasing doses of digitonin even decreased the solubilization yield. At the intermediate concentration of 1.5% digitonin, only half of the membranes had been solubilized (Fig. 3). The Chl *a/b* ratio in the fractions was similar to that of the entire thylakoids of origin (Table 1).

The thylakoid protein profile in the fractions was compared qualitatively using SDS-PAGE (Supplementary Material Fig. S1). In the digitonin-BTH-soluble fraction, LHCII was expectedly abundant (see Ferroni et al., 2016) and explained the relatively low Chl *a/b* ratio. Interestingly, in the corresponding insoluble fraction bands assignable to PSI and ATP synthase subunits were still present. Conversely, the unreliable distribution of PSII subunits between digitonin-ACA-soluble and -insoluble fractions was indicative of an artefactual reorganization of the photosynthetic complexes.

### 3.4. Thylakoid ultrastructure and morphometrics

In cross section, the microphyll of *S. martensii* was formed by three tissues: a monolayer of upper epidermal cells, sparse parenchyma cells of the mesophyll, and a monolayer of lower epidermal cells (Fig. 4A). With respect to the entire plastid area of the leaf sections, the giant chloroplasts hosted in the upper epidermal cells represented 84.8 ± 1.6%, the chloroplasts of the mesophyll 11.8 ± 1.1%, and the chloroplasts of the lower epidermis 4.1 ± 1.1% (mean with SD of $N = 5$ samples).

At the end of the night, in the upper epidermal cells of *S. martensii* the giant chloroplast was cup-shaped and laid at the cell bottom, opposite to the large vacuole (Fig. 4B). Despite several hours of darkness and opposite to expectations, the organelle was still filled with many starch granules. Different from previous observations, no thylakoid dimorphism could be observed between the upper and lower region of the chloroplast, without any trace of the upper elongated lamellae (Ferroni et al., 2016). The very abundant thylakoid system was exclusively organized in grana stacks connected by stroma thylakoids all over the organelle and quite uniformly distributed around the starch granules (Fig. 4C). The same granal organization was observed in the disk-like chloroplasts of the other cell layers, in which starch granules were likewise present (Fig. 4D-F).

**Table 1**
The chlorophyll *a/b* molar ratio (Chl *a/b*) in the detergent-soluble and insolubilized fraction of thylakoids isolated from *Selaginella martensii* at the end of the night and treated with different detergents. Thylakoid membranes were solubilized with different concentrations of β-dodecyl maltoside (β-DM) in bis-tris-HCl (BTH) buffer, or digitonin in BTH, or digitonin in aminocaproic acid buffer (ACA). The insolubilized membranes were pelleted by centrifugation. For each treatment, the weighted mean between the two fractions was calculated based on the yields of solubilization as in Figure 3. The results are means of $N = 3$–5 independent experiments, with SD. Asterisk marks a significant difference between the two fractions according to Student's *t*-test with $P < 0.05$.

| Sample | Chl *a/b* in Solubilized fraction | Chl *a/b* in Non-solubilized fraction | Weighted mean |
|---|---|---|---|
| *Solubilization with β-DM in BTH buffer* | | | |
| Thylakoids | | 2.55 ± 0.07 | |
| BTH - 0% β-DM | | 2.56 ± 0.06 | |
| BTH - 0.75% β-DM | 2.54 ± 0.04 | 2.45 ± 0.13 | 2.53 ± 0.02 |
| BTH - 1.5% β-DM | 2.54 ± 0.07 | 2.28 ± 0.36 | 2.51 ± 0.10 |
| BTH - 2.5% β-DM | 2.52 ± 0.07 | 2.40 ± 0.71 | 2.51 ± 0.06 |
| *Solubilization with digitonin in BTH buffer* | | | |
| Thylakoids | | 2.61 ± 0.17 | |
| BTH - 0% digitonin | | 2.70 ± 0.20 | |
| BTH - 0.75% digitonin | 3.33 ± 0.10 * | 2.39 ± 0.04 | 2.62 ± 0.03 |
| BTH - 1.5% digitonin | 3.13 ± 0.22 * | 2.43 ± 0.03 | 2.59 ± 0.04 |
| BTH - 2.5% digitonin | 3.17 ± 0.24 * | 2.55 ± 0.20 | 2.71 ± 0.18 |
| *Solubilization with digitonin in ACA buffer* | | | |
| Thylakoids | | 2.75 ± 0.04 | |
| ACA - 0% digitonin | | 2.71 ± 0.07 | |
| ACA - 0.75% digitonin | 2.67 ± 0.08 | 2.84 ± 0.34 | 2.70 ± 0.11 |
| ACA - 1.5% digitonin | 2.73 ± 0.07 | 2.78 ± 0.10 | 2.75 ± 0.02 |
| ACA - 2.5% digitonin | 2.82 ± 0.07 | 2.73 ± 0.16 | 2.75 ± 0.12 |

At a first glance, in the upper epidermis chloroplasts, the degree of thylakoid appression was high, but the size of the grana stacks was extremely heterogeneous (Fig. 5A). In the same organelle, grana stacks formed by tens of thylakoid layers were found along with small stacks of only a few layers (Fig. 5A). Giant grana formed by several tens of thylakoid layers were infrequent (an example is reported in Fig. 5B). In some cases, the granum appeared as an individual regular unit well separated from the neighbouring grana (Fig. 5B). The appressed domains of the thylakoids faced each other at the dark grana partitions, which occupied the granum core (Fig. 5C). The non-appressed domains included mainly the stroma thylakoids and the top and bottom layers of each stack (end membranes). Laterally, the continuity domains of the granal thylakoid layers with the stroma lamellae in the region interfacing the appressed and non-appressed membranes, i.e., the grana margins, were well visible (Fig. 5C; Rantala et al., 2020). However, in most cases, the grana appeared quite irregular in shape, particularly because of the shift of the thylakoid layers in the lateral plane (Fig. 5D). Moreover, it was sometimes difficult to identify the borders of each individual stack: a continuity from one stack to the other was mediated by groups of very long appressed thylakoid layers (Fig. 5E). Some particularly complex morphologies of grana stacks could be observed, in which some stroma thylakoids connected distant appressed regions the same granum, somewhat appearing like "embedded" in the granum structure (Fig. 5F). Similar aspects were observed in the chloroplasts of the other microphyll tissues (examples are reported in Supplementary Material Fig. S2). When the grana were sectioned tangentially, the grana layers were visible as disk-shaped structures, and neighbouring disks tended to overlap (Fig. 5G, Supplementary Fig. S2).

The quantitative analysis of the thylakoid system was performed on the giant chloroplasts of the upper epidermis and in the chloroplasts of the mesophyll; the chloroplasts of the lower epidermis, representing only 4% of the plastid area in leaf sections, were not analysed. The thylakoid morphometrics were focussed on selected areas at a magnification offering a good compromise between rich-in-thylakoid field and sufficient resolution of the membranes, sectioned parallel to the stack axis. An accurate way of expressing the degree of thylakoid appression is based on the length of the membranes, which includes the granum perimeter in the calculation of the non-appressed domains. In *S. martensii* the appressed/non-appressed domain ratio was 2.11 ± 0.11 ($N = 24$) and 2.24 ± 0.16 ($N = 24$) in the giant epidermal and disk-shaped mesophyll chloroplasts, respectively and without significant differences between the two tissues, indicating the uniformity of the thylakoid appression within the microphyll (means with SE; Student's *t*-test, $P = 0.52$). The values were lower than expected for plants adapted to the deep shade (4–5) (Anderson et al., 1988). The ratio can be reformulated as a percentage of non-appressed domains: 33.2% ± 1.2% ($N = 24$) and 31.6% ± 1.7% ($N = 10$) in the two tissues, respectively. Taking into account the different area covered in leaf sections by the two types of chloroplasts, the weighted mean was determined as 33.0%, which is higher than the estimate of ca. 24% from the selective solubilization of the non-appressed domains with digitonin (Student's *t*-test between all determinations with either method, $P < 10^{-4}$).

A set of morphometric parameters was calculated to characterize the grana. The granum height *h* and the number *N* of thylakoid layers per stack describe the granum according to the vertical perspective (Fig. 6A). Spanning in the range of $N = [3–48]$, the average of 15 and the median of 14 thylakoids per granum, corresponding to *h* of ca. 250 nm, fell within the range of the granum size normally reported in the literature (5–25, Rantala et al., 2020; Kirchhoff, 2019; Fig. 6B-C). Cases of stacks formed by more than 25 thylakoids, such as that documented in Fig. 5B, were a relatively rare occurrence (less than 10%). The Stacking Repeat Distance *SRD* was found in the range of [13–22] nm, with an average of ca. 17 nm, in line with literature reports in a variety of angiosperms (see Dekker and Boekema, 2005; Fig. 6D). The values obtained for *N* and *h* in the mesophyll chloroplasts did not differ significantly (*h* and *N*) from those of the giant chloroplasts; *SRD* was minimally smaller (ca. 16.4 nm, Student's *t*-test, $P < 0.05$; Supplementary Fig. S3).

As discussed by Mazur et al., a granum stack can be formed by different diameters of the layers and their shift on the lateral plane further complicates the determination (Mazur et al., 2021). Therefore, the horizontal perspective of grana was analysed measuring the length of each thylakoid layer forming each stack; given the size variability of the grana stacks, to obtain a reliable estimate of the granum diameter, we averaged all 932 measured thylakoid layers lengths. The length of the grana layers was distributed in the wide range of [242–1916] nm with a median of 716 nm and a coefficient of variation of 29%; the average length was 733 ± 7 nm (mean with SE; Fig. 7A). A value higher than the theoretical threshold of 500 nm for the granum diameter (Höhner et al., 2020 and reference therein) was found with a frequency of 87%. In the mesophyll chloroplasts, the average length of the granum layers was significantly shorter by 5.6%, but still very high, 692 ± 9 nm (Student's *t*-test, $P < 0.01$; Supplementary Fig. S3). The weighted mean of the granum diameters was 728 nm. The granum irregularity was

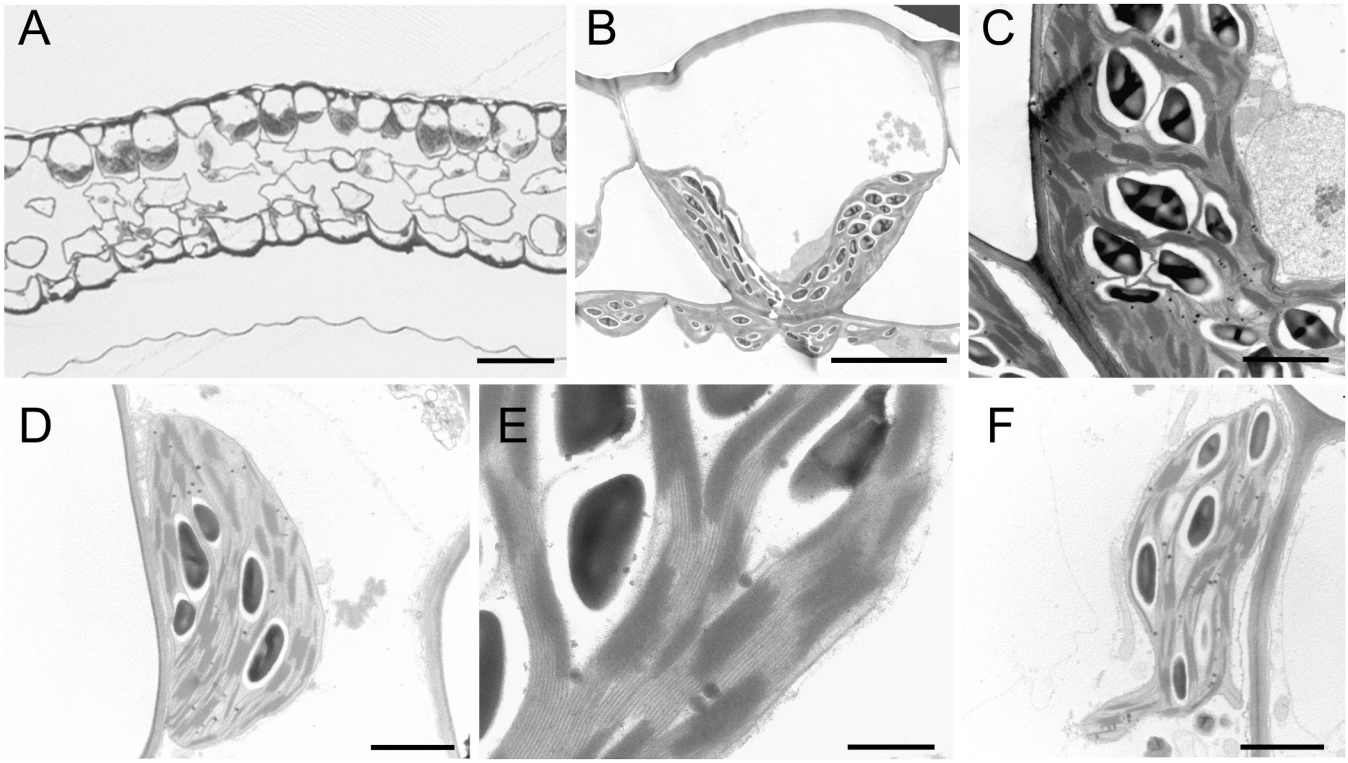


**Fig. 4.** Chloroplasts in the microphyll of *Selaginella martensii* at the end of the night. (A) Cross-section of a microphyll, showing the cell layers of the upper epidermis, the mesophyll and the lower epidermis. (B) A cell of the upper epidermis showing the cup-shaped giant chloroplast. (C) In the giant chloroplast, the thylakoid system is abundant and organized in grana stacks; electron-dense starch granules occupy a large part of the stroma. (D) A disk-shaped chloroplast of the mesophyll. (E) Detail of the granal thylakoid system and starch granules in a mesophyll chloroplast. (F) A chloroplast in a lower epidermal cell. Scale bars: (A) 40 μm; (B) 10 μm; (C-D, F) 2 μm; (E) 0.5 μm.

quantified using the two indexes proposed by Mazur et al., whose meaning is schematized in Fig. 7B (Mazur et al., 2021). The *GLI* index focuses on the irregularity of the thylakoids building one single granum, with a minimum value of 0 when all layers have the same diameter. Clearly, *GLI* can be calculated only in grana sectioned almost perfectly parallel to the vertical granum axis. Analysis of 45 grana in the giant epidermal chloroplasts produced an average GLI of 0.21 ± 0.01 (mean with SE; Fig. 7C). However, *GLI* is not sensitive to the lateral shift of the layers on the lateral plane, which was instead quantified using *GSI*. Particularly, the shifting of the layers, which exposes a larger surface of their membrane to the stroma, gives rise to positive and increasing values of *GSI*. Only in a few cases, the *GSI* values calculated for *S. martensii* giant chloroplasts indicated regular stacks (*GSI* close to 0), while the most frequent occurrence was *GSI* of ca. 0.27 (median; Fig. 7D). The average *GSI* of 0.32 ± 0.03 (mean with SE) was higher than the median and indicated that almost half of the grana were very irregular. Given that the grana occurred in *S. martensii* in a wide range of vertical size, we checked whether the granum irregularity was in relation with the number of thylakoid layers per granum. No correlation was found between *N* and *GLI*, while it was very significant between *N* and *GSI*, indicating that the degree of thylakoid shifting increased with the vertical granum size (Fig. 7E, F). The same properties related to the granum irregularity were found for the mesophyll chloroplasts (Supplementary Fig. S3).

## 4. Discussion

Within the lineage of Viridiplantae, starting from a seeming random alternation of appressed and non-appressed thylakoid domains in green algae, the three-dimensional architecture of the thylakoid system evolved in land plants and originated the highly structured multiple membrane layers known as grana (Gunning and Schwartz, 1999, Gu et al., 2022). However, the granum structure formed by thylakoid membranes with the same diameter and almost perfectly aligned laterally to build a cylinder (Staehelin and Paolillo, 2020) is an idealization, which does not account for the irregular grana shapes observed in most plant species (Mazur et al., 2021; Mustárdy and Garab, 2003). The structural diversity of the thylakoid system in vascular plants has long been interpreted in terms of adaptation to the growth light regime (sun-to-shade gradient; Anderson et al., 1988; 2012). Very interestingly, as compared to euphyllophytes, the sister clade of lycophytes has explored an extreme variability of chloroplast structures, particularly through the species belonging to Selaginellaceae (Liu et al. 2020). The limitations of the granum structural model are evident from the properties of the thylakoid system in the chloroplast of *Selaginella martensii*.

Paradigm of the shade adaptation of the thylakoid system, as derived mainly from angiosperms, is the high membrane extension associated with the enhancement of thylakoid stacking, which is meant in the vertical granum perspective, i.e., a high number of stacked thylakoid layers per granum up to the construction of giant grana (Anderson et al., 1973, 2012; Demmig-Adams et al., 2015; Lichtenthaler and Babani, 2004; Shao et al., 2014). Giant grana have also been documented in a shade-tolerant cycadophyte (Medeghini Bonatti and Fornasiero Baroni, 1990) and in an extreme-shade fern species (Nasrulhaq-Boyce and Duckett, 1991). Interestingly, despite the shade adaptation and the night incubation, in *S. martensii* the occurrence of giant grana is only sporadic. Regular size stacks largely prevail, in line with morphometrics previously reported for the related, shade-tolerant species *S. erythropus* (Sheue et al., 2007). Nonetheless, the Chl *a*/*b* and PSI/PSII ratios are clear biochemical markers of the deep-shade adaptation of *S. martensii* thylakoids. A PSI/PSII ratio of 0.31 is lower than values reported for angiosperms grown in a far-red-enriched environment (0.4–0.5; Fan et al. 2007) but higher than that of grana preparations (0.125–0.25; Danielsson et al., 2004, Koochak et al., 2019). Although our EPR

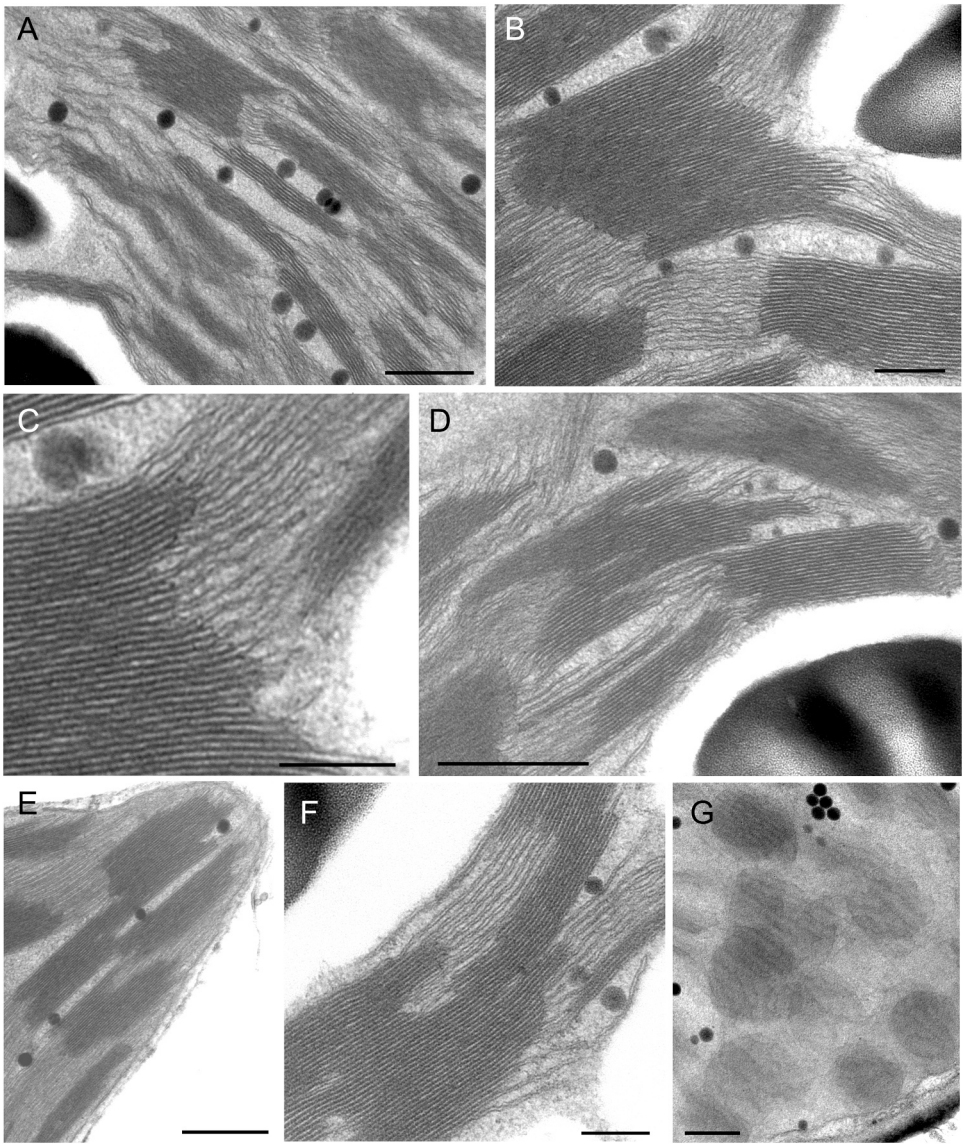


**Fig. 5.** Electron micrographs of the thylakoid system in the giant chloroplast of *Selaginella martensii* at the end of the night. (A) Heterogeneity of the thylakoid stacking extent exemplified by the different height of grana in the same field of observation. (B) One of the few observed examples of a granum with several tens of appressed thylakoids. (C) A detail of the granum border (from granum in B), showing the grana margins alternating with curvature areas. (D) In the centre of the micrograph, a very irregular granum showing extensive shift of the thylakoid layers in the lateral plane. (E) An example of a very irregular granum stack, in which extremely long layers are visible. (F) Detail of an irregular granum; note that some parallel stroma thylakoids connect two distant portions of the same granum, being nearly "embedded" inside the granum. (G) A section tangential to the grana stacks shows the individual disks representing the thylakoid layers; note that the disks tend to largely overlap. Scale bars: (A, D, E, G) 0.5 μm; (B, C, F) 0.2 μm.

determination can be affected by errors due to the small concentration of reaction centres in *S. martensii* thylakoids, the very low PSI/PSII ratio is independently supported by the Chl *a* prompt fluorescence transient, featuring a minute amplitude of the I-P phase: $\Delta V_{I\text{-}P}$ around 0.10 were reported in sciaphilous angiosperms, such as rainforest bromeliads (Martins et al., 2021; Souza et al., 2019). Therefore, *S. martensii* thylakoids exhibit typical biochemical hallmarks of shade adaptation.

Contrasting with the structural paradigm of thylakoid shade-adaptation in angiosperms, *S. martensii* privileges the increase in the granum diameter in place of the increase in the number of layers building the granum. A geometrical feature, somehow grounding the cylindrical granum model of angiosperms, is the very narrow variation range of the thylakoid disk diameter, consistently reported in a range of 400–600 nm (Anderson et al., 2008). This principle, mainly derived from model species, can be easily generalized to (deep) shade-tolerant angiosperms, including those developing giant grana (see a short overview in Supplementary Table S1). Using *Arabidopsis thaliana* mutants lacking thylakoid curvature factors, Höhner et al. (2020) showed that oversized appressed domains cause a restricted plastocyanin diffusion from cytochrome $b_6f$ to PSI. Accordingly, they interpret the restriction of the granum diameter to less than 500 nm as the result of a strong evolutionary pressure facilitating the linear electron flow. A mean granum diameter of 594–680 nm as in *S. erythropus* (Sheue et al., 2007) and even more of 728 nm in *S. martensii* — in both species including grana diameters as long as 1000 nm — demonstrates that exceptions to the 500-nm threshold are possible. Likewise, noticeable exceptions also exist in monilophytes (ferns; Supplementary Table S1, particularly Nasrulhaq-Boyce and Duckett, 1991). Therefore, the evolutionary trajectory fixing the threshold for the lateral development of grana to 500 nm seems specific to angiosperms, and cannot be generalized to seedless euphyllophytes and lycophytes. Nonetheless, in agreement with Höhner et al. (2020), our analysis of $P700^+$ reduction kinetics confirms that a large granum diameter, while very likely emphasises light harvesting, limits the long-range diffusion of plastocyanin, making the re-reduction of P700 very slow. Therefore, the overall thylakoid function in *Selaginella* chloroplasts will require compensation for the slowness of the linear electron flow determined by structural constraints. For example, the high capacity of thermal dissipation of excess absorbed energy documented in *S. martensii* and quite unusual for a deep-shade species can be considered one such mechanism (Ferroni et al., 2014; 2018; 2021; Colpo et al. 2022).

If we aim at a less reductionist representation of *S. martensii* thylakoid system, going beyond the mere grana-intergrana antithesis, electron micrographs suggest a particularly complex three-dimensionality of

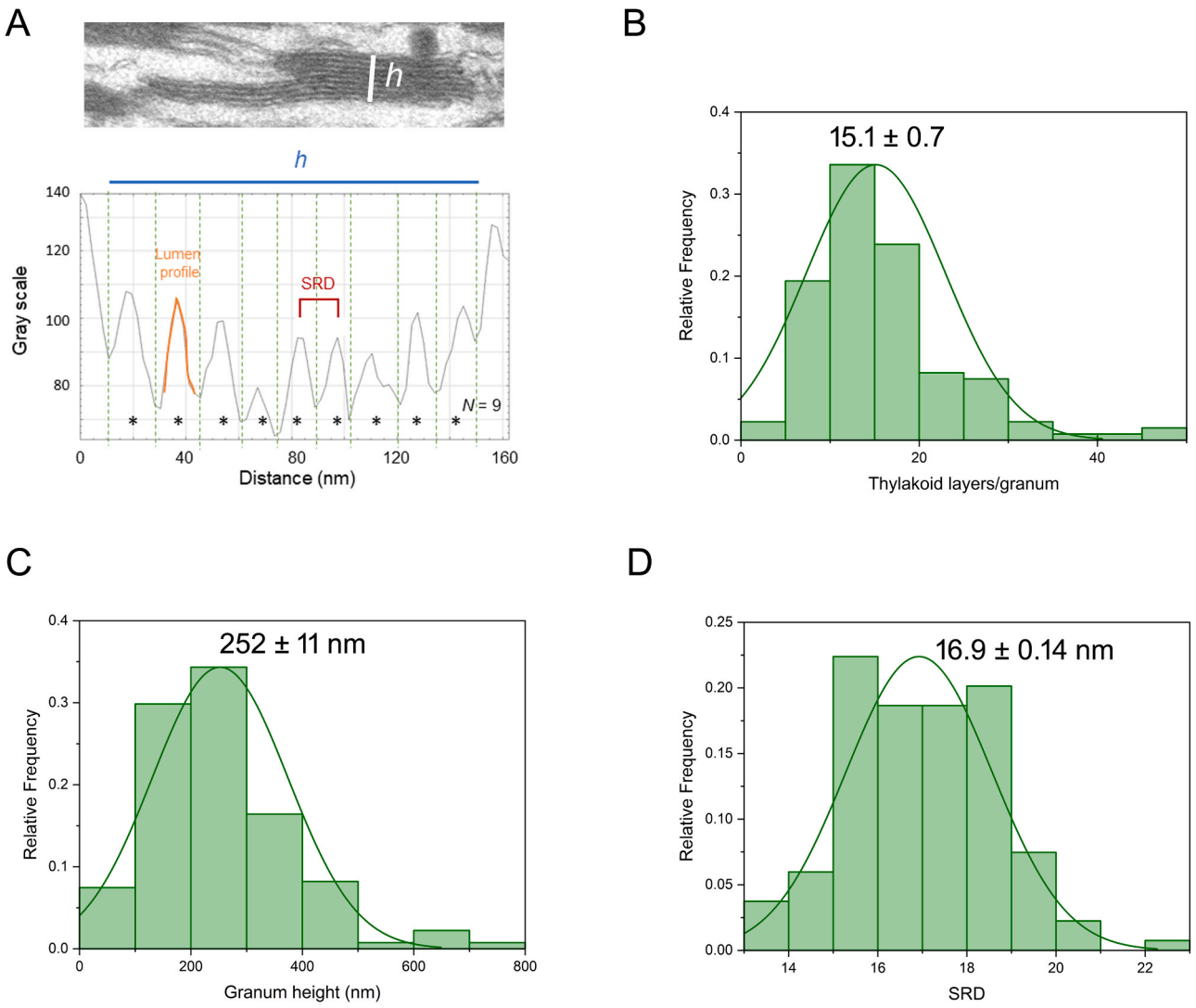


**Fig. 6.** Vertical granum morphometrics in the giant chloroplasts of the upper epidermis of *S. martensii* leaf. (A) Scheme of the measured parameters for the example of the shown granum. The grey scale profile, obtained with the ImageJ Plot Profile function, shows the height *h* of the stack (distance between the top and bottom end-membranes) and outlines the lumen profiles. By counting the number *N* of layers (asterisks), the Stacking Repeat Distance *SRD* is calculated. (B-D) Histograms of the parameters, each reported with the corresponding normal distribution and mean value ± SE (134 grana analysed from 24 micrographs taken from 4 independent plants).

the thylakoid architecture in *S. martensii*. Mazur et al. recently recalled that the cylindric granum model does not catch the complexity of grana in angiosperms, where irregularity is more the rule than the exception (Mazur et al., 2021). Views of the thylakoid system in *Selaginella* species exemplifies how relevant this caveat is in a lycophyte (Ferroni et al., 2016; Ghaffar et al., 2018; Jagels, 1970; Liu et al., 2020; Sheue et al., 2007). The characterization of a granum irregularity considers two aspects: the variability of the disk diameters and the lateral sliding apart of the thylakoid layers, quantified by *GLI* and *GSI*, respectively (Kowalewska et al., 2016; Mazur et al., 2021). In *S. martensii*, we calculated *GLI*= 0.21 and *GSI*= 0.32, but how do these values compare with those of other shade species? To obtain an indication, we calculated the two indexes in a set of published chloroplast micrographs, including *S. erythropus*, *S. apoda* and the non-shade-adapted lycophyte *Isoetes sinensis* (Jagels, 1970, Ghaffar et al., 2018, Ding et al., 2015). We evidenced a problem with the calculation of GSI in the case oval or trapezoidal grana (e.g., *Anoectochilus roxburghii*, (Shao et al., 2014)), which resulted in negative values; in such cases, the granum was treated as free from lateral sliding of layers, assigning *GSI*= 0. In Supplementary Table S2, the range of variation for the euphyllophytes is *GLI* = [0.09–0.20] and *GSI* = [0–0.33]. The *Selaginella* species, but not *I. sinensis*, tended to lay at the upper limit of the intervals. To quantify comprehensively such irregularity, we introduce the synthetic index $GI_{TOT}$, defined as the sum of *GSI* and *GLI*. The range of variation of $GI_{TOT}$ in euphyllophytes is [0.18–0.42]. In *Selaginella* species, $GI_{TOT} \geq 0.40$ quantifies the higher complexity of the thylakoid system as compared to other species (Fig. 8). Therefore, in *S. martensii* the complex thylakoid arrangements visible both in cross- and tangential sections (Fig. 5E-G, S2) result from assembling thylakoid layers of variable width that tend to slide apart from each other as the number of stacked layers increases (Fig. 7F).

The problem of the quantification of the thylakoid appression can be analysed through direct morphometrics of the thylakoid system, or biochemically by exploiting a selective detergent like digitonin. Because of the small hydrophobic moiety represented by the sterol part, the action of digitonin is limited to the outer leaflet of a membrane bilayer (Fan and Heerklotz, 2017). At the same time the hydrophilic oligosaccharidic part is too bulky and cannot penetrate the narrow stromal gaps (Järvi et al., 2011; Suorsa et al., 2015). Consequently, the digitonin-soluble thylakoid fraction can be used to assess quantitatively

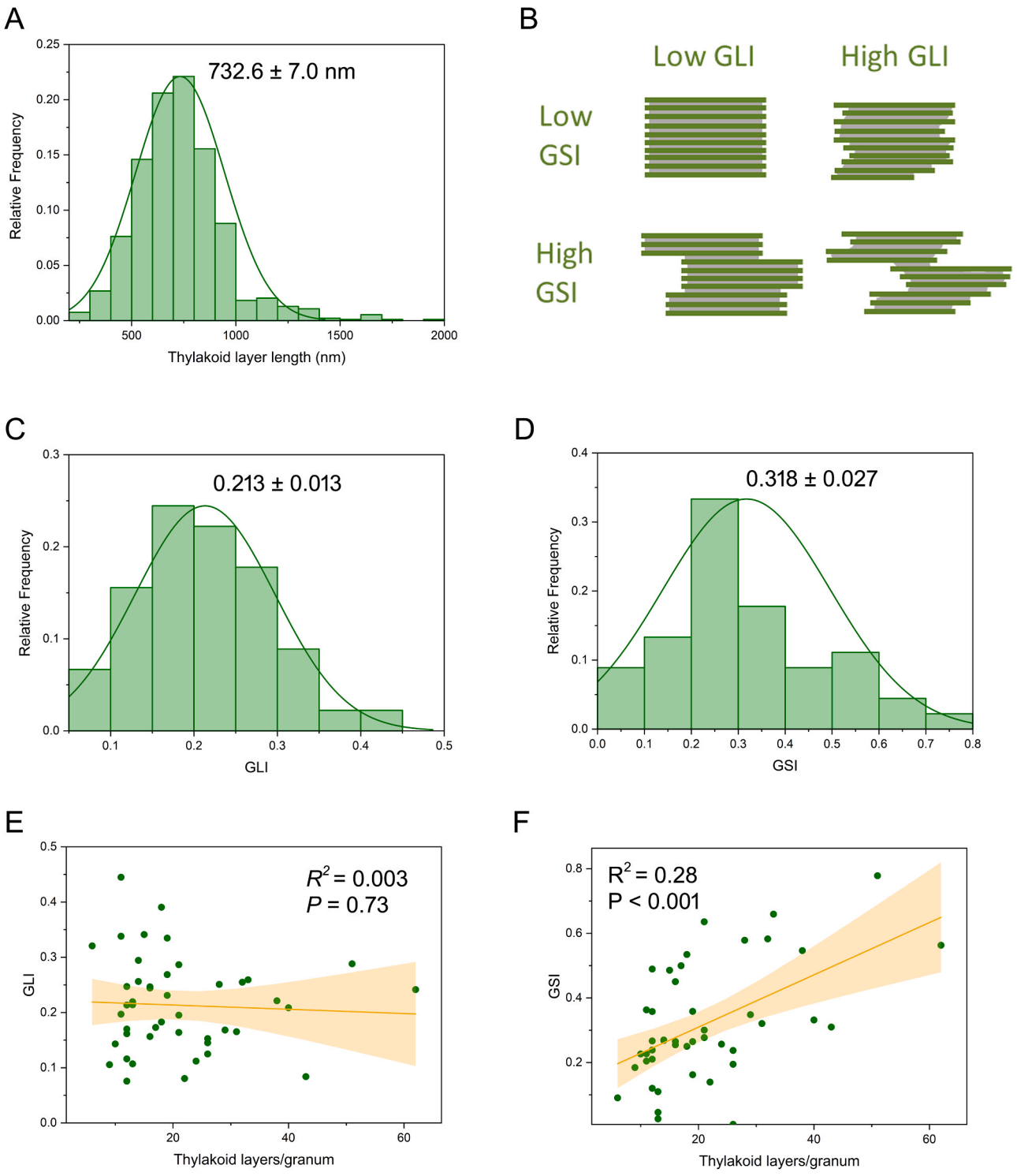


**Fig. 7.** Horizontal granum morphometrics in the giant chloroplasts of the upper epidermis of *S. martensii* leaf. (A) Histograms of the lengths of the grana thylakoid layers with the corresponding normal distribution and mean value ± SE (932 layers analysed from 24 micrographs taken from 4 independent plants). (B) Schematic representation of the granum irregularity according to Mazur et al. (2021). The lateral irregularity (*GLI*) evaluates the deviation from an ideal condition in which all layers have the same length; the cross-sectional irregularity (*GSI*) quantifies the deviation from the ideal cylindrical shape because of lateral shifts of the layers. (C-D) Histograms of *GLI* and *GSI* with the corresponding normal distribution and mean value ± SE (45 grana analysed from 24 micrographs taken from 4 independent plants). (E-F) Co-variation of the number of thylakoid layers per granum with *GLI* or *GSI*. The regression lines with 95% confidence bands, $R^2$ and corresponding *P* values are reported.

the amount of non-appressed membranes (Rantala et al., 2017). Interestingly, we have found a discrepancy by 9% between the quantification of the non-appressed domains using the biochemical or morphometric method, i.e., 24% vs 33%, respectively. The difference, besides being statistically significant ($P < 10^{-4}$, Student's *t*-test), is not negligible and indicates that about 1/3 of the non-appressed membranes is not solubilized by digitonin. The presence of some PSI and ATP synthase complexes in the digitonin-BTH-insoluble fraction is probably related to the

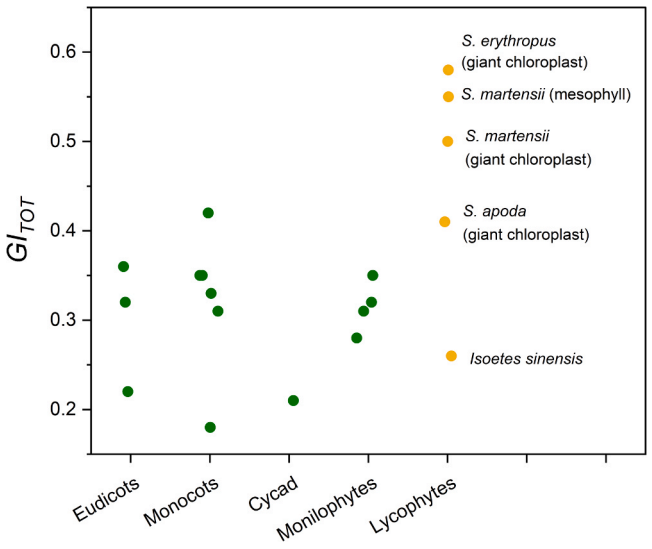


**Fig. 8.** Variability of the irregularity index $GI_{TOT}$ among shade-tolerant species belonging to euphyllophytes (Eudicots, Monocots, Cycads, Monilophytes) and lycophytes.

missing non-appressed domains. The incomplete accessibility of digitonin to the stroma-exposed membranes could depend on the surface charge density and distribution (Chow et al., 2005), which can be related to the abundance of LHCII that characterizes the stroma lamellae in *S. martensii*. In fact, the Chl *a*/*b* ratio in digitonin-BTH-soluble fraction is much lower than expected for stroma thylakoids (3.2 vs. 4.5–7.1; Rantala et al., 2017; Koochak et al., 2019), but it is in line with previous evidence of abundant PSII–LHCII–PSI–LHCI megacomplexes in the same fraction (Ferroni et al., 2016). Moreover, the particularly complex thylakoid network built by irregular grana, as assessed by $GI_{TOT}$, can further hinder the capacity of digitonin penetration. It is not excluded that, under the conditions of solubilisation, some stroma thylakoid regions may adhere locally through the "velcro-like" action of LHCII, which would similarly prevent the digitonin action. The recalcitrancy of the dark-acclimated *S. martensii* thylakoids against the action of digitonin is further confirmed by the unsuccessful results obtained with use of the ACA buffer, which leads instead to a nearly complete membrane solubilization in *Arabidopsis* (Rantala et al., 2020; 2022).

In a comparative perspective, the non-appressed/appressed membrane ratio of ca. 2 and the corresponding stacking degree of 67% (or, less reliably, ca. 3% and 76% based on digitonin) are lower than expected for a shade plant. The method we used is adapted from Jan Anderson's papers and refers to the measurement of membrane lengths; the introduction of the $\delta_{STACK}$ parameter can also lead to some overestimation of the stacking degree. In absolute terms, a stacking degree of 67% is higher than reported values of 50–60% in sun-adapted/acclimated plants, but it is lower than common values found in shade-adapted/acclimated plants, as high as 80–85% (Anderson et al., 1988; Lichtenthaler et al., 1981; Pancaldi et al., 1998). One can speculate that the enhancement in the light-harvesting capacity, which in angiosperms is allowed primarily by increasing the thylakoid stacking degree, in *Selaginella* can be achieved integrating stacking and irregularity of grana. In both cases, and actually in all shade-tolerant vascular species, inside the stroma the grana stacks are oriented in all directions to enable an effective absorption of weak diffuse light (Anderson et al., 1973; Jagels, 1970; Medeghini Bonatti and Fornasiero Baroni, 1990; Nasrulhaq-Boyce and Duckett, 1991). Noticeably, the level of structural complexity of the thylakoid system in *Selaginella* species can be higher than described in this work. A unique thylakoid zonation into elongated lamellae formed by a few thylakoids and, underneath, the granal system is an ultrastructural trait shared by the deep-shade species included in subgenus *Stachygynandrum* (Liu et al., 2020), which includes *S. martensii*. This intra-organelle dimorphism is interpreted as a special adaptation to deep shade and seems a very stable structural feature (Ghaffar et al., 2018; Sheue et al., 2015). In *S. martensii* the absence of the elongated lamellae after a night-long dark incubation was an unexpected finding, and a somehow fortunate event to allow the study in a simplified only-granal system. Interestingly, in their extensive comparative analysis of chloroplasts in *Selaginella* species, Liu et al. (2020) could not find any thylakoid zonation in *S. martensii*. Our observation suggests that the differentiation of the lamellar region is inducible in the short-term in *S. martensii* and requires the exposure to light.

In conclusion, the evolution of chloroplast adaptive traits to deep shade has occurred in parallel in lycophytes and euphyllophytes, up to the most recent lineage of angiosperms. We suggest that, under the same environmental pressure including low light intensity, far red enrichment, and unpredictable sunflecks, the two lineages underwent a convergent evolution of some basic traits, e.g., the extension of the thylakoid system and the enlargement of the antenna complement. However, a closer look also highlights significant elements of divergence, particularly the vertical development of grana in angiosperms and, conversely, the lateral widening of thylakoid appressions in lycophytes, particularly the width of 500 nm is not an upper threshold to the stacked thylakoid diameter in lycophytes, as also in some ferns. The parallel evolution of shade adaptation traits in euphyllophytes and lycophytes is shown to include issues related to the granum irregularity, which can be analysed quantitatively by means of recently introduced parameters.

## Declaration of Competing Interest

The authors declare that they have no known competing financial interests or personal relationships that could have appeared to influence the work reported in this paper.

## Data Availability

Data will be made available on request.

## Acknowledgements

This research received funding from the University of Ferrara through Fondo per l'Incentivazione alla Ricerca - FIR 2020 (granted to L. F.), the project OPVaI-VA/DP/2018/No.313011T813 "Optimization of phenotyping methods: building a national phenotyping platform" (granted to M.B.), the Science Grant Agency of the Slovak Republic no. VEGA 1-0664-22 (granted to M.B.). We are grateful to Fausto Molinari and Roberta Marchesini (Botanical Garden of the University of Ferrara) for taking care of the plants used for experiments, and to Marjaana Rantala (University of Turku, Finland) for her helpful suggestions about thylakoid solubilization.

## Appendix A. Supporting information

Supplementary data associated with this article can be found in the online version at doi:10.1016/j.plantsci.2023.111833.

## References

P. Albanese, S. Tamara, G. Saracco, R.A. Scheltema, C. Pagliano, How paired PSII–LHCII supercomplexes mediate the stacking of plant thylakoid membranes unveiled by structural mass-spectrometry, Nat. Commun. 11 (1) (2020) 1–14.

J.M. Anderson, D.J. Goodchild, N.K. Boardman, Composition of the photosystems and chloroplast structure in extreme shade plants, Biochim. Et Biophys. Acta (BBA)-Bioenerget. 325 (3) (1973) 573–585.

J.M. Anderson, W.S. Chow, D.J. Goodchild, Thylakoid membrane organisation in sun/shade acclimation, Funct. Plant Biol. 15 (2) (1988) 11–26.

J.M. Anderson, W.S. Chow, J. De Las Rivas, Dynamic flexibility in the structure and function of photosystem II in higher plant thylakoid membranes: the grana enigma, Photosynth. Res. 98 (2008) 575–587.
J.M. Anderson, P. Horton, E.H. Kim, W.S. Chow, Towards elucidation of dynamic structural changes of plant thylakoid architecture, Philos. Trans. R. Soc. B: Biol. Sci. 367 (1608) (2012) 3515–3524.
B. Andersson, J.M. Anderson, Lateral heterogeneity in the distribution of chlorophyll-protein complexes of the thylakoid membranes of spinach chloroplasts, Biochim. Et Biophys. Acta (BBA)-Bioenerg. 593 (2) (1980) 427–440.
U. Armbruster, M. Labs, M. Pribil, S. Viola, W. Xu, M. Scharfenberg, et al., *Arabidopsis* CURVATURE THYLAKOID1 proteins modify thylakoid architecture by inducing membrane curvature, Plant Cell 25 (7) (2013) 2661–2678.
E.M. Aro, M. Suorsa, A. Rokka, Y. Allahverdiyeva, V. Paakkarinen, A. Saleem, et al., Dynamics of photosystem II: a proteomic approach to thylakoid protein complexes, J. Exp. Bot. 56 (411) (2005) 347–356.
J.R. Austin, L.A. Staehelin, Three-dimensional architecture of grana and stroma thylakoids of higher plants as determined by electron tomography, Plant Physiol. 155 (4) (2011) 1601–1611.
J. Barber, An explanation for the relationship between salt-induced thylakoid stacking and the chlorophyll fluorescence changes associated with changes in spillover of energy from photosystem II to photosystem I, FEBS Lett. 118 (1) (1980) 1–10.
J. Brangeon, L. Mustárdy, The ontogenetic assembly of intra-chloroplastic lamellae viewed in 3-dimension, Biol. Cell. 36 (1) (1979) 71–80.
Y. Bussi, E. Shimoni, A. Weiner, R. Kapon, D. Charuvi, R. Nevo, et al., Fundamental helical geometry consolidates the plant photosynthetic membrane, Proc. Natl. Acad. Sci. USA 116 (44) (2019) 22366–22375.
M.A. Castillo, W.P. Wardley, M. Lopez-Garcia, Light-dependent morphological changes can tune light absorption in iridescent plant chloroplasts: a numerical study using biologically realistic data, ACS Photonics 8 (4) (2021) 1058–1068.
M.G. Ceppi, A. Oukarroum, N. Çiçek, R.J. Strasser, G. Schansker, The IP amplitude of the fluorescence rise OJIP is sensitive to changes in the photosystem I content of leaves: a study on plants exposed to magnesium and sulfate deficiencies, drought stress and salt stress, Physiol. Plant. 144 (3) (2012) 277–288.
W.S. Chow, E.-H. Kim, P. Horton, J.M. Anderson, Granal stacking of thylakoid membranes in higher plant chloroplasts: the physicochemical forces at work and the functional consequences that ensue, Photochem. Photobiol. Sci. 4 (2005) 1081–1090.
A. Colpo, C. Baldisserotto, S. Pancaldi, A. Sabia, L. Ferroni, Photosystem II photoinhibition and photoprotection in a lycophyte, *Selaginella martensii*, Physiol. Plant. 174 (1) (2022), e13604.
R. Danielsson, P.Å. Albertsson, F. Mamedov, S. Styring, Quantification of photosystem I and II in different parts of the thylakoid membrane from spinach, Biochim. Et Biophys. Acta (BBA)-Bioenerget. 1608 (1) (2004) 53–61.
B. Daum, D. Nicastro, J. Austin, J.R. McIntosh, W. Kühlbrandt, Arrangement of photosystem II and ATP synthase in chloroplast membranes of spinach and pea, Plant Cell 22 (4) (2010) 1299–1312.
J.P. Dekker, E.J. Boekema, Supramolecular organization of thylakoid membrane proteins in green plants, Biochim. Et. Biophys. Acta 1706 (2005) 12–39.
B. Demmig-Adams, O. Muller, J.J. Stewart, C.M. Cohu, W.W. Adams III, Chloroplast thylakoid structure in evergreen leaves employing strong thermal energy dissipation, J. Photochem. Photobiol. B: Biol. 152 (2015) 357–366.
G. Ding, C. Li, X. Han, C. Chi, D. Zhang, B. Liu, Effects of lead on ultrastructure of *Isoetes sinensis* Palmer (Isoetaceae), a critically endangered species in China, PLoS One 10 (9) (2015), e0139231.
M. Ermakova, C. Bellasio, D. Fitzpatrick, R.T. Furbank, F. Mamedov, S. von Caemmerer, Upregulation of bundle sheath electron transport capacity under limiting light in C4 *Setaria viridis*, Plant J. 106 (5) (2021) 1443–1454.
D.Y. Fan, A.B. Hope, P.J. Smith, H. Jia, R.J. Pace, J.M. Anderson, W.S. Chow, The stoichiometry of the two photosystems in higher plants revisited, Biochim. Et Biophys. Acta (BBA)-Bioenerget 1767 (8) (2007) 1064–1072.
H.Y. Fan, H. Heerklotz, Digitonin does not flip across cholesterol-poor membranes, J. Colloid Interface Sci. 504 (2017) 283–293.
L. Ferroni, A. Colpo, C. Baldisserotto, S. Pancaldi, In an ancient vascular plant the intermediate relaxing component of NPQ depends on a reduced stroma: Evidence from dithiothreitol treatment, J. Photochem. Photobiol. B: Biol. 215 (2021), 112114.
L. Ferroni, M. Suorsa, E.M. Aro, C. Baldisserotto, S. Pancaldi, Light acclimation in the lycophyte *Selaginella martensii* depends on changes in the amount of photosystems and on the flexibility of the light-harvesting complex II antenna association with both photosystems, New Phytol. 211 (2) (2016) 554–568.
L. Ferroni, M. Angeleri, L. Pantaleoni, C. Pagliano, P. Longoni, F. Marsano, et al., Light-dependent reversible phosphorylation of the minor photosystem II antenna Lhcb6 (CP 24) occurs in lycophytes, Plant J. 77 (6) (2014) 893–905.
L. Ferroni, S. Cucuzza, M. Angeleri, E.M. Aro, C. Pagliano, M. Giovanardi, et al., In the lycophyte *Selaginella martensii* is the "extra-qT" related to energy spillover? Insights into photoprotection in ancestral vascular plants, Environ. Exp. Bot. 154 (2018) 110–122.
L. Ferroni, M. Živčak, M. Kovar, A. Colpo, S. Pancaldi, S.I. Allakhverdiev, M. Brestič, Fast chlorophyll a fluorescence induction (OJIP) phenotyping of chlorophyll-deficient wheat suggests that an enlarged acceptor pool size of Photosystem I helps compensate for a deregulated photosynthetic electron flow, J. Photochem. Photobiol. B: Biol. 234 (2022), 112549.
A. Filacek, M. Zivcak, M. Barboricova, S.P. Misheva, E.G. Pereira, X. Yang, M. Brestic, Diversity of responses to nitrogen deficiency in distinct wheat genotypes reveals the role of alternative electron flows in photoprotection, Photosynth. Res. 154 (3) (2022) 259–276.
G. Garab, Self-assembly and structural–functional flexibility of oxygenic photosynthetic machineries: personal perspectives, Photosynth. Res. 127 (2016) 131–150.
R. Ghaffar, M. Weidinger, B. Mähnert, M. Schagerl, I. Lichtscheidl, Adaptive responses of mature giant chloroplasts in the deep-shade lycopod *Selaginella erythropus* to prolonged light and dark periods, Plant Cell Environ. 41 (8) (2018) 1791–1805.
K.S. Gould, D.W. Lee, Physical and ultrastructural basis of blue leaf iridescence in four Malaysian understory plants, Am. J. Bot. 83 (1) (1996) 45–50.
M. Grieco, M. Suorsa, A. Jajoo, M. Tikkanen, E.M. Aro, Light-harvesting II antenna trimers connect energetically the entire photosynthetic machinery—including both photosystems II and I, Biochim. Et Biophys. Acta (BBA)-Bioenerget 1847 (6–7) (2015) 607–619.
L. Gu, B. Grodzinski, J. Han, T. Marie, Y.J. Zhang, Y.C. Song, Y. Sun, Granal thylakoid structure and function: explaining an enduring mystery of higher plants, New Phytol. 236 (2) (2022) 319–329.
B.E.S. Gunning, O.M. Schwartz, Confocal microscopy of thylakoid autofluorescence in relation to origin of grana and phylogeny in the green algae, Funct. Plant Biol. 26 (7) (1999) 695–708.
Y. Guo, Y. Lu, V. Goltsev, R.J. Strasser, H.M. Kalaji, H. Wang, et al., Comparative effect of tenuazonic acid, diuron, bentazone, dibromothymoquinone and methyl viologen on the kinetics of Chl a fluorescence rise OJIP and the MR820 signal, Plant Physiol. Biochem. 156 (2020) 39–48.
R. Höhner, M. Pribil, M. Herbstová, L.S. Lopez, H.H. Kunz, M. Li, et al., Plastocyanin is the long-range electron carrier between photosystem II and photosystem I in plants, Proc. Natl. Acad. Sci. USA 117 (26) (2020) 15354–15362.
R. Jagels, Photosynthetic apparatus in *Selaginella*. II. Changes in plastid ultrastructure and pigment content under different light and temperature regimes, Can. J. Bot. 48 (10) (1970) 1853–1860.
S. Järvi, M. Suorsa, V. Paakkarinen, E.M. Aro, Optimized native gel systems for separation of thylakoid protein complexes: novel super-and mega-complexes, Biochem. J. 439 (2) (2011) 207–214.
D. Killi, A. Raschi, F. Bussotti, Lipid peroxidation and chlorophyll fluorescence of photosystem II performance during drought and heat stress is associated with the antioxidant capacities of C3 sunflower and C4 maize varieties, Int. J. Mol. Sci. 21 (14) (2020) 4846.
H. Kirchhoff, Chloroplast ultrastructure in plants, New Phytol. 223 (2) (2019) 565–574.
C. Klughammer, U. Schreiber, Saturation pulse method for assessment of energy conversion in PS I, Planta 192 (1994) 261–268.
H. Koochak, S. Puthiyaveetil, D.L. Mullendore, M. Li, H. Kirchhoff, The structural and functional domains of plant thylakoid membranes, Plant J. 97 (3) (2019) 412–429.
L. Kowalewska, R. Mazur, S. Suski, M. Garstka, A. Mostowska, Three-dimensional visualization of the tubular-lamellar transformation of the internal plastid membrane network during runner bean chloroplast biogenesis, Plant Cell 28 (2016) 875–891.
T.T. Kozlowski, S.G. Pallardy, Growth Control in Woody Plants, Elsevier, 1997.
U.K. Laemmli, Cleavage of structural proteins during the assembly of the head of bacteriophage T4, Nature 227 (5259) (1970) 680–685.
H.K. Lichtenthaler, F. Babani, Light adaptation and senescence of the photosynthetic apparatus. Changes in pigment composition, chlorophyll fluorescence parameters and photosynthetic activity. Chlorophyll *a* fluorescence: A signature of Photosynthesis, Springer, Dordrecht, 2004, pp. 713–736.
H.K. Lichtenthaler, C. Buschmann, M. Döll, H.-J. Fietz, T. Bach, U. Kozel, D. Meier, U. Rahmsdorf, Photosynthetic activity, chloroplast ultrastructure, and leaf characteristics of high-light and low-light plants and of sun and shade leaves, Photosynth. Res. 2 (1981) 115–141.
J.W. Liu, S.F. Li, C.T. Wu, I.A. Valdespino, J.F. Ho, Y.H. Wu, et al., Gigantic chloroplasts, including bizonoplasts, are common in shade-adapted species of the ancient vascular plant family *Selaginellaceae*, Am. J. Bot. 107 (4) (2020) 562–576.
J.P.R. Martins, S.W. Moreira, P.C.S. Braga, L.T. Conde, R. Cipriano, A.R. Falqueto, A.B.P. L. Gontijo, Photosynthetic apparatus performance and anatomical modulations of *Alcantarea imperialis* (Bromeliaceae) exposed to selenium during in vitro growth, Photosynthetica 59 (4) (2021) 529–537.
N.J. Masters, M. Lopez-Garcia, R. Oulton, H.M. Whitney, Characterization of chloroplast iridescence in *Selaginella erythropus*, J. R. Soc. Interface 15 (148) (2018), 20180559.
S. Mathur, L. Jain, A. Jajoo, Photosynthetic efficiency in sun and shade plants, Photosynthetica 56 (1) (2018) 354–365.
R. Mazur, A. Mostowska, Ł. Kowalewska, How to measure grana–ultrastructural features of thylakoid membranes of plant chloroplasts, Front. Plant Sci. 12 (2021).
P. Medeghini Bonatti, R. Fornasiero Baroni, Developmental pattern and structural organisation of leaf chloroplasts in *Lepidozamia peroffskyana*, Aust. J. Bot. 38 (1990) 53–62.
K.R. Miller, L.A. Staehelin, Analysis of the thylakoid outer surface. Coupling factor is limited to unstacked membrane regions, J. Cell Biol. 68 (1) (1976) 30–47.
L. Mustárdy, G. Garab, Granum revisited. A three-dimensional model – where things fall into place, Trends Plant Sci. 8 (3) (2003) 117–122.
L. Mustárdy, K. Buttle, G. Steinbach, G. Garab, Three-dimensional architecture of the granum-stroma thylakoid membrane system revealed by electron tomography, in: J. F. Photosynthesis, E. Allen, J.H. Gantt, B. Golbeck, Osmond (Eds.), Photosynthesis. Energy from the Sun: 14th International Congress on, Springer, Heidelberg, Germany, 2008a, pp. 771–774.
L. Mustárdy, K. Buttle, G. Steinbach, G. Garab, The three-dimensional network of the thylakoid membranes in plants: quasihelical model of the granum-stroma assembly, The Plant Cell (2008b) 2552–2557.
A. Nasrulhaq-Boyce, J.G. Duckett, Dimorphic epidermal cell chloroplasts in the mesophyll-less leaves of an extreme–shade tropical fern, *Teratophyllum rotundifoliatum* (R. Bonap.) Holtt.: a light and electron microscope study, New Phytol. 119 (1991) 433–444.

R. Nevo, D. Charuvi, O. Tsabari, Z. Reich, Composition, architecture and dynamics of the photosynthetic apparatus in higher plants, Plant J. 70 (1) (2012) 157–176.
S. Pancaldi, A. Bonora, R. Gualandri, R. Gerdol, R. Manservigi, M.P. Fasulo, Intra-tissue characteristics of chloroplasts in the lamina and petiole of mature winter leaf of *Arum italicum* Miller, Bot. Acta 111 (4) (1998) 261–272.
L. Pantaleoni, L. Ferroni, C. Baldisserotto, E.M. Aro, S. Pancaldi, Photosystem II organisation in chloroplasts of *Arum italicum* leaf depends on tissue location, Planta 230 (5) (2009) 1019–1031.
S.H. Pao, P.Y. Tsai, C.I. Peng, P.J. Chen, C.C. Tsai, E.C. Yang, et al., Lamelloplasts and minichloroplasts in Begoniaceae: iridescence and photosynthetic functioning, J. Plant Res. 131 (4) (2018) 655–670.
M. Pollastrini, V. Holland, W. Brüggemann, H. Bruelheide, I. Dănilă, B. Jaroszewicz, et al., Taxonomic and ecological relevance of the chlorophyll a fluorescence signature of tree species in mixed European forests, N. Phytol. 212 (1) (2016) 51–65.
M. Pollastrini, E. Salvatori, L. Fusaro, F. Manes, R. Marzuoli, G. Gerosa, et al., Selection of tree species for forests under climate change: is PSI functioning a better predictor for net photosynthesis and growth than PSII? Tree Physiol. 40 (11) (2020) 1561–1571.
M. Rantala, M. Tikkanen, E.M. Aro, Proteomic characterization of hierarchical megacomplex formation in *Arabidopsis* thylakoid membrane, Plant J. 92 (5) (2017) 951–962.
M. Rantala, S. Rantala, E.M. Aro, Composition, phosphorylation and dynamic organization of photosynthetic protein complexes in plant thylakoid membrane, Photochem. Photobiol. Sci. 19 (5) (2020) 604–619.
M. Rantala, A. Ivanauskaite, L. Laihonen, S.D. Kanna, B. Ughy, P. Mulo, Chloroplast acetyltransferase GNAT2 is involved in the organization and dynamics of thylakoid structure, Plant Cell Physiol. 63 (9) (2022) 1205–1214.
G. Schansker, S.Z. Tóth, R.J. Strasser, Methylviologen and dibromothymoquinone treatments of pea leaves reveal the role of photosystem I in the Chl a fluorescence rise OJIP, Biochim. Et Biophys. Acta (BBA)-Bioenerget. 1706 (3) (2005) 250–261.
M.A. Schöttler, S.Z. Tóth, Photosynthetic complex stoichiometry dynamics in higher plants: environmental acclimation and photosynthetic flux control, Front. Plant Sci. 5 (2014) 188.
Q. Shao, H. Wang, H. Guo, A. Zhou, Y. Huang, Y. Sun, M. Li, Effects of shade treatments on photosynthetic characteristics, chloroplast ultrastructure, and physiology of *Anoectochilus roxburghii*, PLoS One 9 (2) (2014), e85996.
C.R. Sheue, V. Sarafis, R. Kiew, H.Y. Liu, A. Salino, L.L. Kuo-Huang, et al., Bizonoplast, a unique chloroplast in the epidermal cells of microphylls in the shade plant *Selaginella erythropus* (Selaginellaceae), Am. J. Bot. 94 (12) (2007) 1922–1929.
C.R. Sheue, J.W. Liu, J.F. Ho, A.W. Yao, Y.H. Wu, S. Das, et al., A variation on chloroplast development: the bizonoplast and photosynthetic efficiency in the deep-shade plant *Selaginella erythropus*, Am. J. Bot. 102 (4) (2015) 500–511.
M.C. Shih, P.J. Xie, J. Chen, P. Chesson, C.R. Sheue, Size always matters, shape matters only for the big: potential optical effects of silica bodies in *Selaginella*, J. R. Soc. Interface 19 (192) (2022), 20220204.
A.F.C. Souza, J.P.R. Martins, A.B.P.L. Gontijo, A.R. Falqueto, Selenium improves the transport dynamics and energy conservation of the photosynthetic apparatus of in vitro grown *Billbergia zebrina* (Bromeliaceae), Photosynthetica 57 (4) (2019) 931–941.
L.A. Staehelin, D.J. Paolillo, A brief history of how microscopic studies led to the elucidation of the 3D architecture and macromolecular organization of higher plant thylakoids, Photosynth. Res. 145 (3) (2020) 237–258.
A. Stirbet, Govindjee, On the relation between the Kautsky effect (chlorophyll *a* fluorescence induction) and photosystem II: basics and applications of the OJIP fluorescence transient, J. Photochem. Photobiol. B: Biol. 104 (2011) 236–257.
M. Suorsa, M. Rantala, F. Mamedov, M. Lespinasse, A. Trotta, M. Grieco, et al., Light acclimation involves dynamic re-organization of the pigment–protein megacomplexes in non-appressed thylakoid domains, Plant J. 84 (2) (2015) 360–373.
S.Z. Tóth, G. Schansker, R.J. Strasser, A non-invasive assay of the plastoquinone pool redox state based on the OJIP-transient, Photosynth. Res. 93 (1) (2007) 193–203.
A. Trotta, A.A. Bajwa, I. Mancini, V. Paakkarinen, M. Pribil, E.M. Aro, The role of phosphorylation dynamics of CURVATURE THYLAKOID 1B in plant thylakoid membranes, Plant Physiol. 181 (4) (2019) 1615–1631.
M. Tsimilli-Michael, Revisiting JIP-test: An educative review on concepts, assumptions, approximations, definitions and terminology, Photosynthetica 58 (2020) 275–292.
M. Umar, Z. Uddin, Z.S. Siddiqui, Responses of photosynthetic apparatus in sunflower cultivars to combined drought and salt stress, Photosynthetica 57 (2) (2019) 627–639.
R.G. Walters, P. Horton, Acclimation of *Arabidopsis thaliana* to the light environment: changes in composition of the photosynthetic apparatus, Planta 195 (2) (1994) 248–256.
S. Weststrand, P. Korall, A subgeneric classification of *Selaginella* (Selaginellaceae), Am. J. Bot. 103 (12) (2016) 2160–2169.
M. Zivcak, M. Brestic, H.M. Kalaji, Govindjee, Photosynthetic responses of sun-and shade-grown barley leaves to high light: is the lower PSII connectivity in shade leaves associated with protection against excess of light? Photosynth. Res. 119 (3) (2014b) 339–354.
M. Zivcak, H.M. Kalaji, H.B. Shao, K. Olsovska, M. Brestic, Photosynthetic proton and electron transport in wheat leaves under prolonged moderate drought stress, J. Photochem. Photobiol. B: Biol. 137 (2014a) 107–115.
M. Zivcak, M. Brestic, K. Kunderlikova, K. Olsovska, S.I. Allakhverdiev, Effect of photosystem I inactivation on chlorophyll a fluorescence induction in wheat leaves: does activity of photosystem I play any role in OJIP rise? J. Photochem. Photobiol. B: Biol. 152 (2015) 318–324.